Moving Solid Metallic Targets for Pion Production in the Muon Collider / Neutrino Factory Project

P.A. Thieberger and H.G. Kirk
Brookhaven National Laboratory

Introduction

The production of large fluxes of pions and muons using high energy, high intensity proton pulses impinging on solid or liquid targets[1)] presents unique problems which have not yet been entirely solved. The large required power and power density deposited in the material as well as the short pulse duration produce large, almost instantaneous local heating, and the resulting sudden thermal expansion can result in damage-causing stresses in solids and in the violent disruption of liquid jets.

So far three types of target materials have been proposed and investigated to some extent, both theoretically and experimentally. They are steel, graphite and mercury with the largest recent emphasis on the last two. While none of these alternatives can be ruled out at this point, we will briefly mention below some of the problems observed[2)] and envisaged with mercury[3)] and graphite[4)], which provided the incentive for the present, new and more detailed look at high strength steel and Invar alloys.

During a recent series of experiments[2)] with 24 GeV proton pulses hitting both stationary and moving mercury targets, we observed the dispersal of the liquid targets with beam pulses up to 4 TP (less than the 16 TP and 34 TP pulses required for the 1 MW and 4 MW options to be discussed). While the dispersal velocity was seen to be modest enough to mitigate concerns for damage to the interior of the target vessel, new concerns arose [3)] that the residual mercury drops within the target chamber will not sufficiently clear the vessel. The mercury jet will be flowing at about 2 liters per second and much of this mercury, following the interaction with the beam, will collide with the walls and remain in the target chamber before settling into the pool of mercury which will serve as the beam dump. This residual material could interfere with the produced pions spiraling within the solenoidal capture system and with subsequent portions of the mercury jet.

The recently measured[2)], extremely small, beam-induced strains in a carbon-carbon composite indicate that such a material may perhaps survive the thermal shock induced by a much more intense beam. Since these targets are envisaged as being stationary one must consider the problem of removing the power deposited by the beam without interfering too much with the particles being extracted. Recent estimates[4)] indicate that the average temperatures reached by these targets will exceed the range where the linear expansion coefficient is sufficiently small. However other special high-strength graphites[4)], somewhat similar to the ATJ carbon used in the experiments[2)] may actually work. Insufficient data is available at present for a full evaluation.

The conditions created by the short beam pulses (rms width ~50 ns during recent tests[2)] and <5 ns for the final system[1)]) are very unusual. Intense almost instantaneous beam heating causes a fraction of the target volume to suddenly be in a highly compressed, inertially confined state. Subsequently this volume expands initiating strong vibrations in the material. The amplitude of these oscillations is such that large negative pressures (tension) or shear stresses can be generated exceeding the strength of the material and thus causing mechanical damage. To evaluate this situation in detail for a given geometrical configuration and a given material, extensive computer simulations are required such as the ones recently performed[5)] for the windows in experiment E951[2)].

Here we attempt to develop simple, more general criteria, suitable for a preliminary screening of possible materials by evaluating their relative merits. Computer modeling will still be required once a candidate material is selected and specific target geometries are considered. The two criteria we will discuss are:

1) Assume that negative pressures (tension) will arise in the oscillations which are similar in magnitude to the initial compression.

2) Assume that the compressive energy initially available can appear later in a similar volume (same energy density) as tensile energy available to do damage.

Both criteria may be violated if significant vibration focusing effects take place such as were observed in calculations[5] for circular windows rigidly constrained at their periphery. We will assume here that such highly symmetric geometries with natural foci can be avoided by adopting appropriate target geometries, thus avoiding such situations. In fact the natural tendency in most cases should be for the energy initially concentrated in a fraction of the target volume to rapidly spread over the entire volume thus reducing subsequent peak values. Before describing and further justifying these criteria we first evaluate the characteristic vibration periods and heat transfer times in the target materials.

Characteristic Times

The times over which energy is deposited by the beam are of the order of ~50 ns rms for the recent E951 experiment [2] and ~5 ns for the proposed facility [1] The nature of the phenomena and of the approximations we can make depend on how these times compare with the thermal time constant of the target and the vibrational period or sound transit time across the diameter of the target[6].

The results for sound transit times shown for iron in Fig. 1 correspond to a radial sound velocity of 5100 m/s, which is within ± 2% of values for different types of steel.[7].

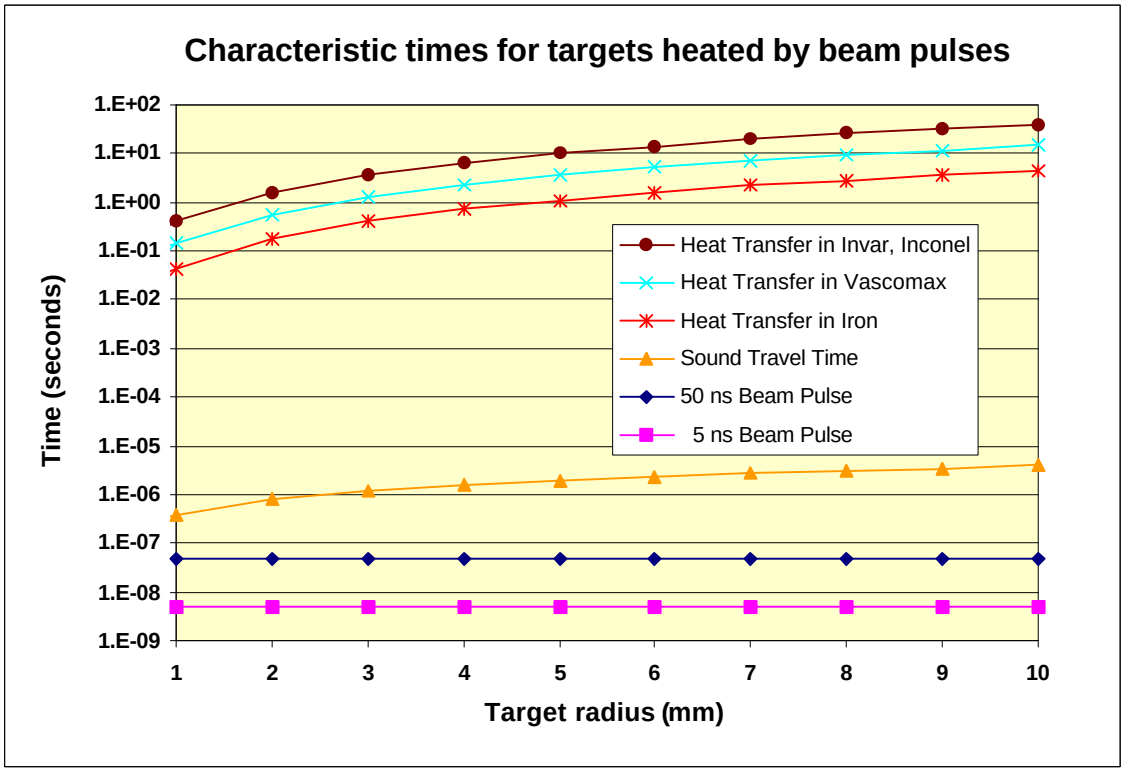

Fig. 1 The sound travel times are the same within ±2% for the materials considered here and the value used for the velocity is 5100 m/s. The order-of-magnitude heat transfer times are 1/e decay times for the exponential decay of a temperature difference across a characteristic distance equal to the radius of the target.

We see from fig. 1 that the sound transit times and therefore the oscillation periods are much longer than the 5ns beam pulse length planned for the final system. For example for a 5 mm radius target the ratio of these times is 392.

Or, looking at this in another way, for a velocity of 5100 m/s the distance traveled by the disturbance in 5 ns is only 25.5 μm compared to a beam size of several mm. Therefore, to a very good approximation, nothing moves appreciably during the pulse and the thermal expansion is inertially confined, leading to a large initial compression.

Large temperature differences will arise inside the target following a beam pulse. The time it takes for such temperature differences to decay will depend on the gradients, the specific heat c_p and the thermal conductivity κ of the material. Here we only make rough order-of-magnitude estimates to determine whether or not heat conduction will play a significant role in the time interval after the pulse during which large vibrational stresses may occur. For this purpose we replace our target by an infinite sheet of thickness r (equal to the radius), into one side of which flows a constant heat flux ϕ, the other side being attached to a heat sink maintained at temperature T_0 which will receive a flux $\phi' = \phi$ .The temperature T of the input side will then be such that:

$$\phi = \kappa \times (T - T_0) / r \qquad 1)$$

If we now suddenly turn off the input heat flux, ϕ' will initially stay at its previous value but will start to decrease as the object cools down. The initial rate of this cooling, dT_{av}/dt, will depend on the heat capacity per unit area $c_p \times \rho \times r$ of the sheet, where ρ is the density :

$$dT_{av}/dt = \phi / (c_p \times \rho \times r) = \kappa \times (T - T_0) / (c_p \times \rho \times r^2) \qquad 2)$$

The rate of decay of a temperature difference across any object of characteristic dimension r is proportional to that temperature difference, with a constant of proportionality roughly equal to $\sim \kappa / (c_p \times \rho \times r^2)$. The inverse of this quantity , $c_p \times \rho \times r^2 / \kappa$, i.e. the 1/e decay time, is plotted as the upper three curves of Fig.1.

We see that not only will single oscillations be adiabatic, but heat conduction will not be a significant factor even after hundreds of oscillations.

Criteria for Selecting a Material

The most straightforward comparison for evaluating a material for this application is between the value of the initial compression and the yield stress or the fatigue limit. A symmetric compression is of course not the primary cause of damage, but the idea is that, as the vibrations evolve, the Fourier components of the initial pressure pulse may later recombine generating tensions of the same order of magnitude. We will later address the limitations of this criterion. In any case it should provide a rough idea of the suitability, and a reasonable comparison between the relative merits of various materials.

To determine the initial compression we must first find values of the energy density deposited by the beam. This was done by using the MARS code[8)] for a number of different iron target radii, and by assuming a beam σ 2.5 times smaller in each case. An example of such a calculation is shown in Fig. 2 for a target radius of 7.5 mm, a beam rms radius of 3 mm and a proton pulse of 16 TP (1TP = 10^{12} protons.)

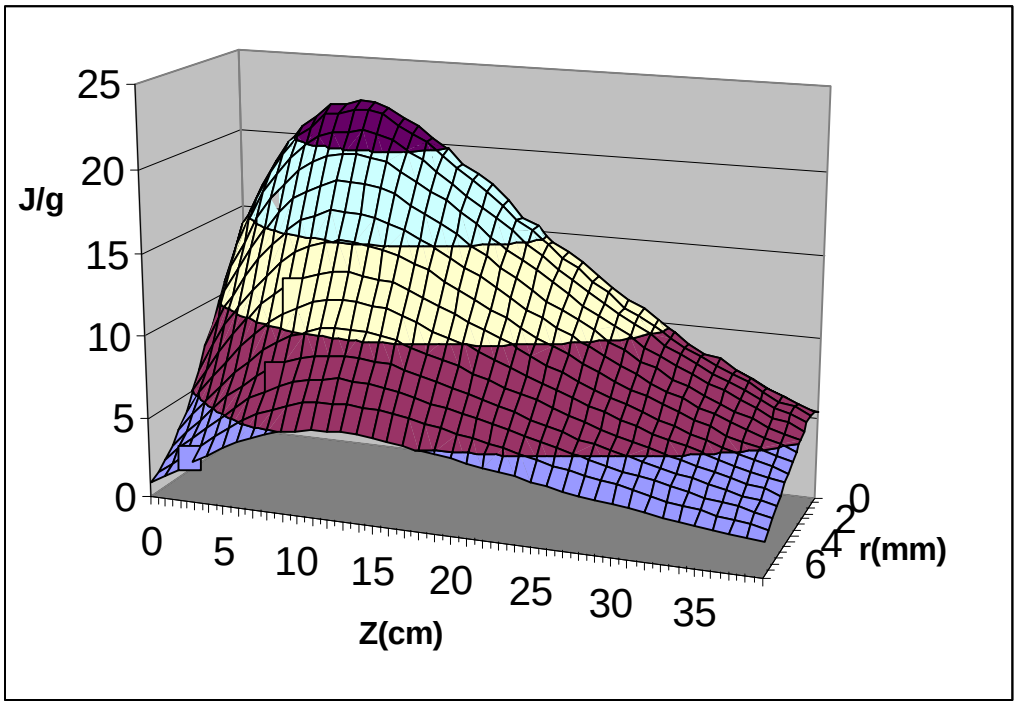

Fig. 2 Three-dimensional view of energy deposition MARS data for a 3 mm rms radius 16TP beam on a 7.5 mm radius iron target.

The result of these MARS calculations for iron are summarized in Table 1

Table 1. Maximum energy density deposited by a 16TP, 24 GeV beam in an iron target.

Beam width [rms mm]	.5	1	1.5	2	2.5	3	3.5
Target radius [mm]	1.25	2.5	3.75	5	6.25	7.5	8.75
Maximum energy density [J/g]	305	105	55.6	36.0	26.5	22.1	16.5

These calculations are time consuming, and the values obtained for iron are representative enough for the alloys considered here since the densities are similar and the atomic number of the main constituents cover a relatively narrow range (see Table 3). Once the maximum value ε_{max} of the energy density (per unit mass) is found from these calculations for each case we calculate the corresponding maximum compression P_{max} for each material.

$$P_{max} = 3 \times \varepsilon_{max} \times B \times \alpha / c_v \qquad 3)$$

Where B is the bulk modulus, α the linear expansion coefficient and c_v the specific heat at constant volume. Values for these parameters, and for others used later are listed in Table 2 for the materials of interest. The chemical compositions of these alloys are detailed in Table 3.

Table 2. Mechanical an thermal characteristics of the materials

	Density	Linear Exp. Coeff.	Young Modulus	Bulk Modulus	Poisson Ratio	Specific Heat @ constant pressure	Thermal Conductivity	Yield Strength	Fatigue Endurance Limit
Symbol	ρ	α	Y	B	μ	c_p	λ	$\sigma_{0.2}$	σ_{-1}
Unit	g/cm^3	10^{-6} / ^{0}K	G Pa	G Pa		J/(g ^{0}K)	W/(m ^{0}K)	M Pa	M Pa
Iron	7.87	12.5	205	171	0.30	0.478	80	170	~85
Inconel 718	8.19	13.1	200	158	0.29	0.435	11.2	1034	586
VascoMax C-350	8.08	15.0	200	167	0.30	0.450	25.2	2242	758
Super Invar	8.15	0.63	144	88.9	0.23	0.515	10.5	276	~138

Table 3. Typical Chemical Compositions (%).

Element	C	Al	Si	S	Ti	Cr	Mn	Fe	Co	Ni	Cu	Nb	Mo
Atomic Number	6	13	14	16	22	24	25	26	27	28	29	41	42
Inconel 718		0.5			1	19		19		52.5		5	3
Vasco Max C-350	.02	0.1	.05	.005	1.4		.05	63	12	18.5			4.8
Super Invar	.05	.07	.09	.01		.03	.4	62	5.4	31.8	.08		

We consider the second criterion mentioned above because the effects of oscillations along the three axes are not really independent, and because "mode mixing" is possible, i.e. initial oscillations along the y-axis, for instance, can later contribute to the amplitude along the y-axis. Such effects are included in detailed computer simulations for each particular geometry. To arrive at a general criterion, we first calculate the energy E_σ per unit volume required to stress the material to reach the yield stress $\sigma_{0.2}$ or the fatigue endurance limit σ_{-1} :

$$E_\sigma = \sigma^2 / (2\,Y) \qquad (4)$$

Where σ is either $\sigma_{0.2}$ or σ_{-1} according to which comparison we want to make. We then compare this energy density to the mechanical energy E_m initially available in the compressed, inertially confined, volume. This is only a fraction of the total energy E_{tot} deposited by the beam, the rest being converted immediately to heat:

$$E_m = E_{tot} \times B \times \alpha^2 \times (2\,T_0 + 3/2\,E_{tot}/c_p) / (c_p \times \rho) \qquad (5)$$

where T_0 is the absolute temperature before beam heating, c_p is the specific heat and ρ is the density.

Derivations of equations 3), 4) and 5) are given in the appendix.

One final comment regarding the above criteria is in order. Our application of these criteria will probably be conservative or pessimistic because values for yield stresses and fatigue endurance limits we will use have all been experimentally determined at frequencies which are orders of magnitude smaller than the hundreds of kHz characteristic of the transverse oscillations of interest here. There is evidence[9] that fatigue endurance limits increase with frequency already at the much lower frequencies used for these tests. The same is probably true for yield stresses which are normally determined under essentially static conditions.

Stress Estimates

The results of the calculations outlined in the previous section are shown in Figs. 3 through 10. Figs. 3 through 6 correspond to the first criterion in terms of maximum compressive stresses as % of yield stress and % of fatigue endurance limit, both for the 1 MW and the 4 MW options. Figs. 7 through 10 correspond to the second criterion in terms of available energy to yield- and fatigue endurance limit ratios, also for the 1 MW and the 4 MW options.

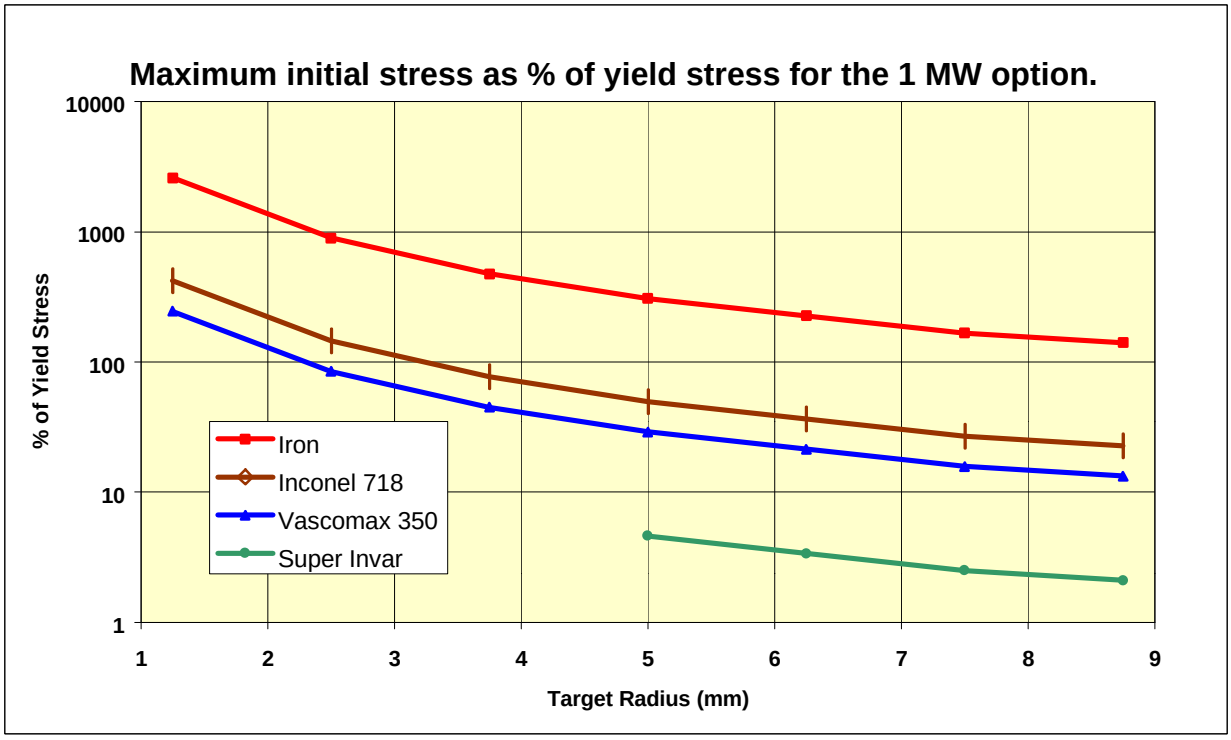
Maximum initial stress as % of yield stress for the 1 MW option.
% of Yield Stress
10000
1000
100
10
1
1
2
3
4
5
6
7
8
9
Target Radius (mm)
Iron
Inconel 718
Vascomax 350
Super Invar

Fig. 3

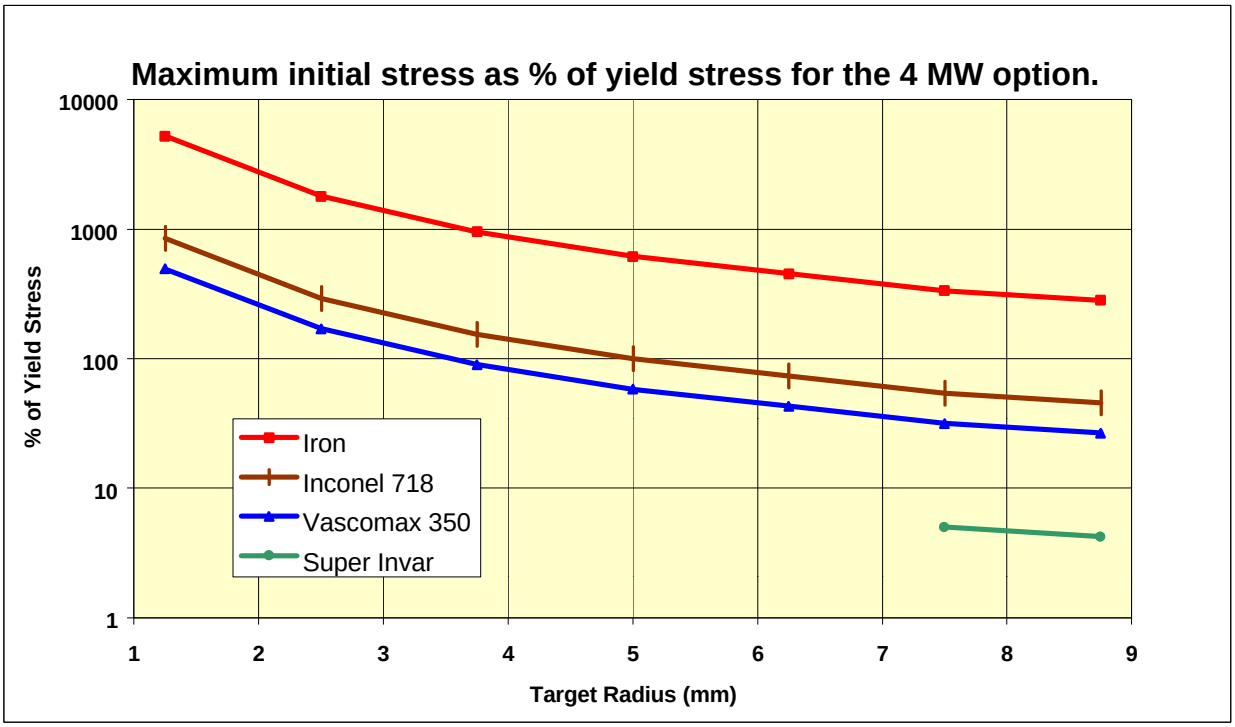
Maximum initial stress as % of yield stress for the 4 MW option.
% of Yield Stress
10000
1000
100
10
1
1
2
3
4
5
6
7
8
9
Target Radius (mm)
Iron
Inconel 718
Vascomax 350
Super Invar

Fig. 4

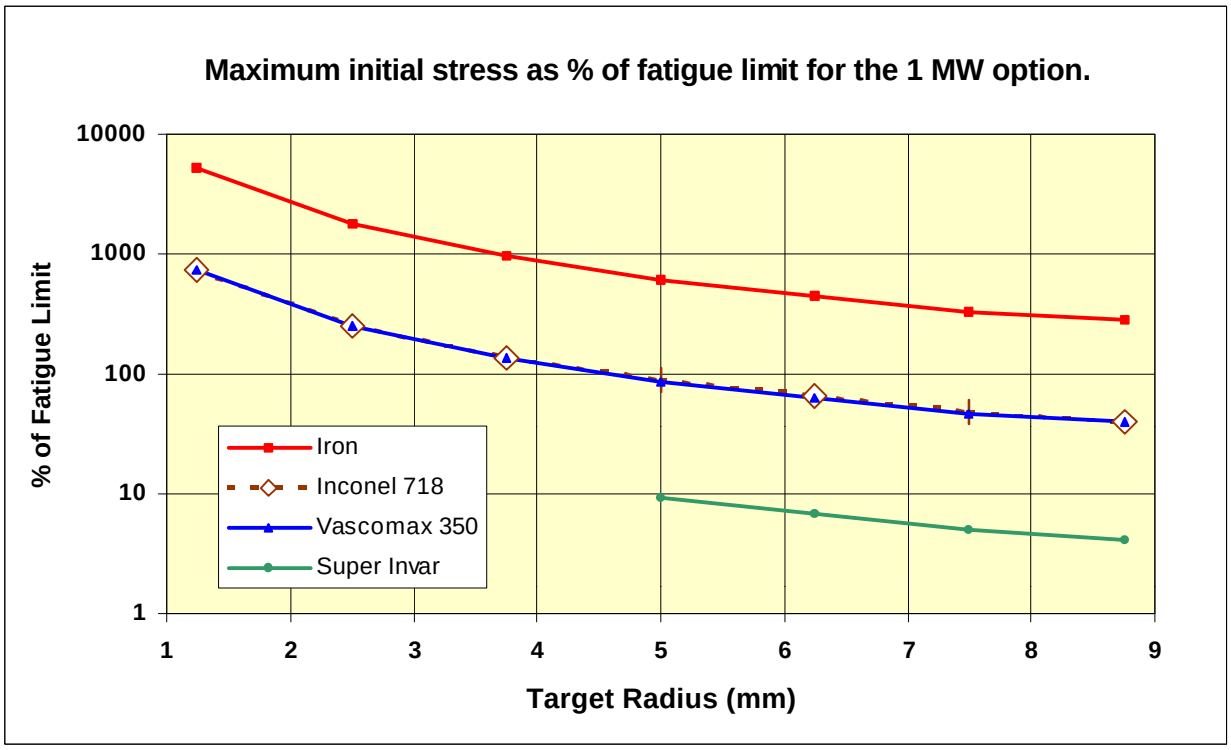
Maximum initial stress as % of fatigue limit for the 1 MW option.
% of Fatigue Limit
10000
1000
100
10
1
1
2
3
4
5
6
7
8
9
Target Radius (mm)
Iron
Inconel 718
Vascomax 350
Super Invar

Fig. 5

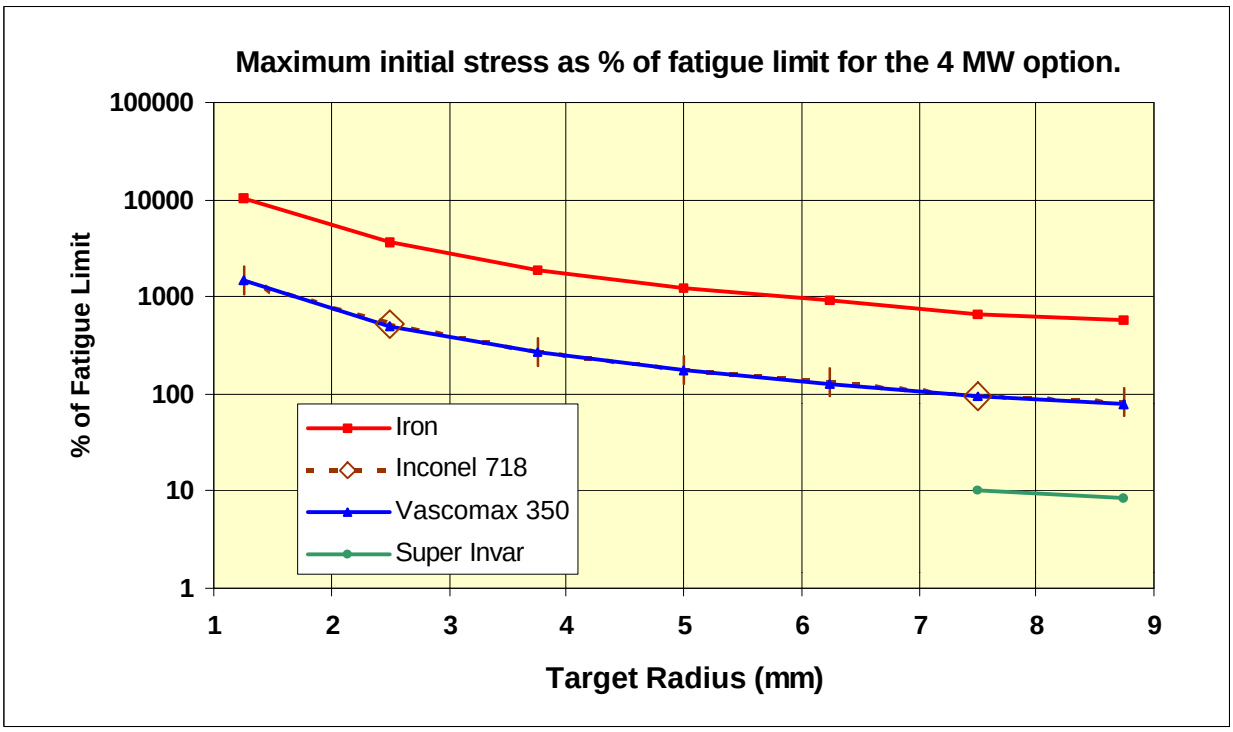
Maximum initial stress as % of fatigue limit for the 4 MW option.
% of Fatigue Limit
100000
10000
1000
100
10
1
1
2
3
4
5
6
7
8
9
Target Radius (mm)
Iron
Inconel 718
Vascomax 350
Super Invar

Fig. 6

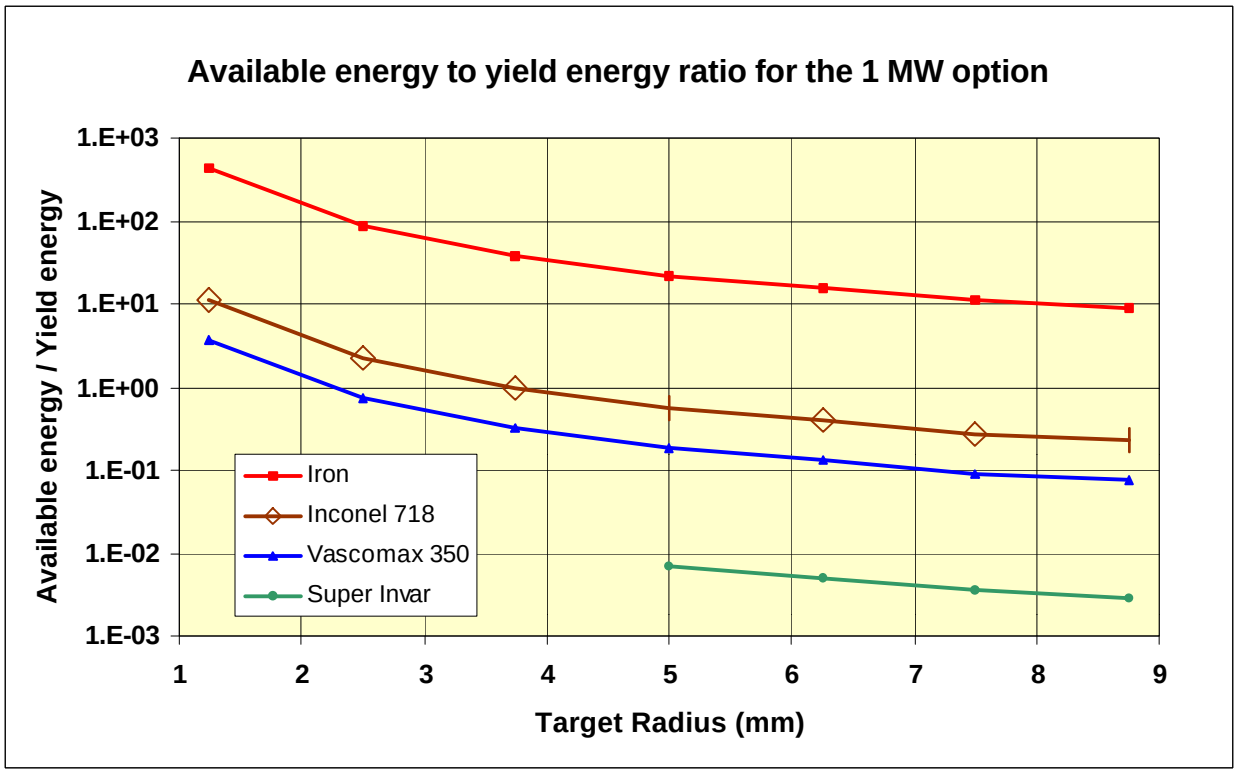
Available energy to yield energy ratio for the 1 MW option
Available energy / Yield energy
1.E+03
1.E+02
1.E+01
1.E+00
1.E-01
1.E-02
1.E-03
1
2
3
4
5
6
7
8
9
Target Radius (mm)
Iron
Inconel 718
Vascomax 350
Super Invar

Fig. 7

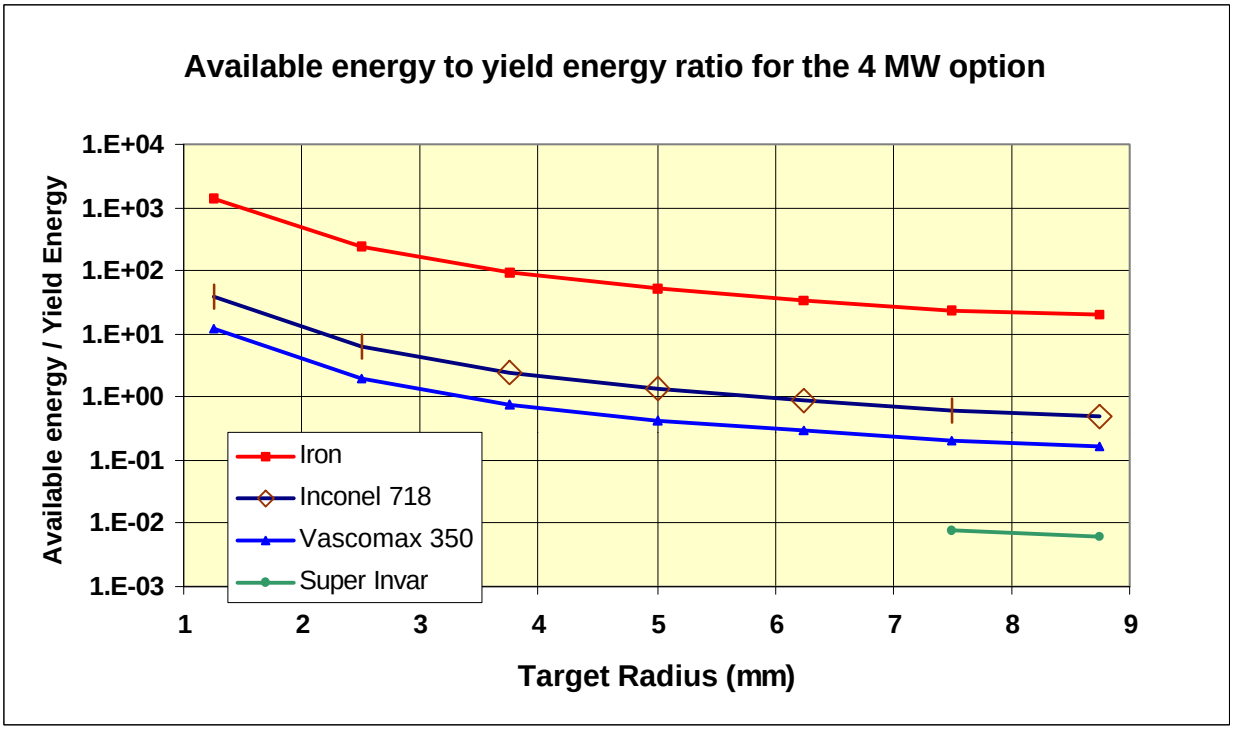
Available energy to yield energy ratio for the 4 MW option
Available energy / Yield Energy
1.E+04
1.E+03
1.E+02
1.E+01
1.E+00
1.E-01
1.E-02
1.E-03
1
2
3
4
5
6
7
8
9
Target Radius (mm)
Iron
Inconel 718
Vascomax 350
Super Invar

Fig 8

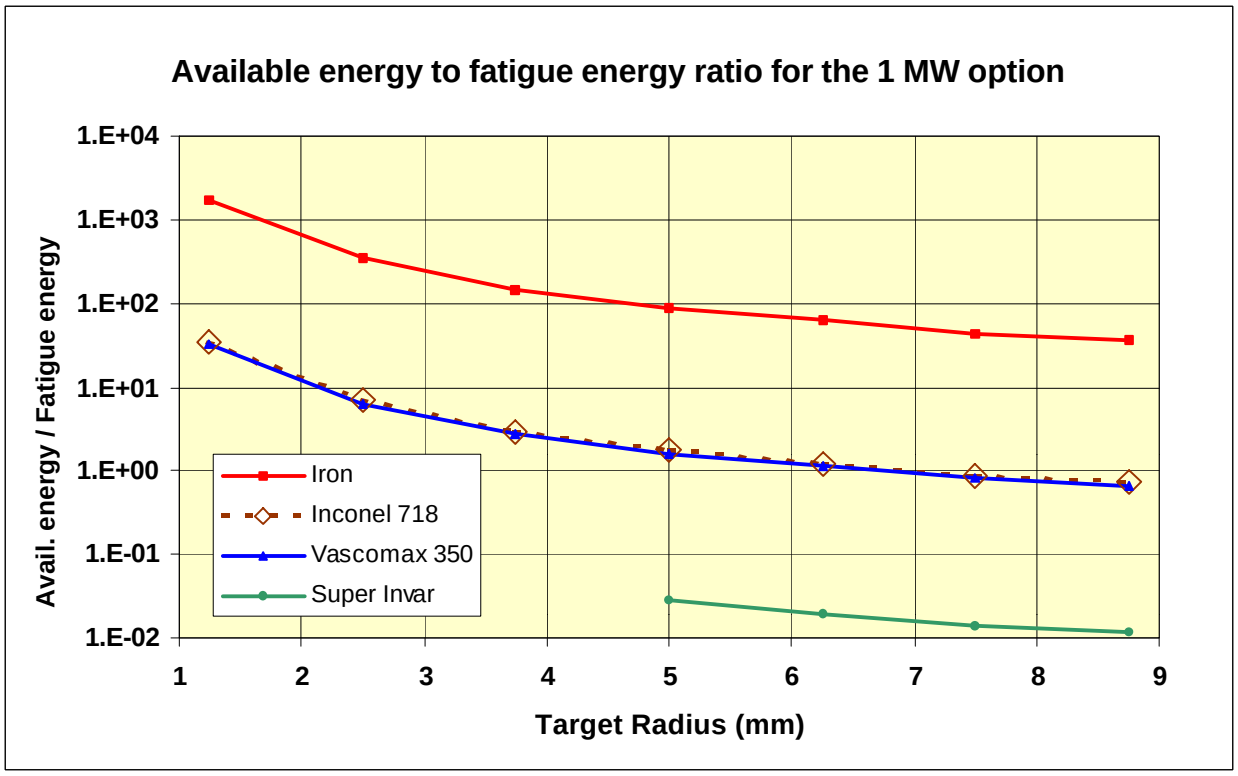
Available energy to fatigue energy ratio for the 1 MW option
Avail. energy / Fatigue energy
1.E+04
1.E+03
1.E+02
1.E+01
1.E+00
1.E-01
1.E-02
1
2
3
4
5
6
7
8
9
Target Radius (mm)
Iron
Inconel 718
Vascomax 350
Super Invar

Fig. 9

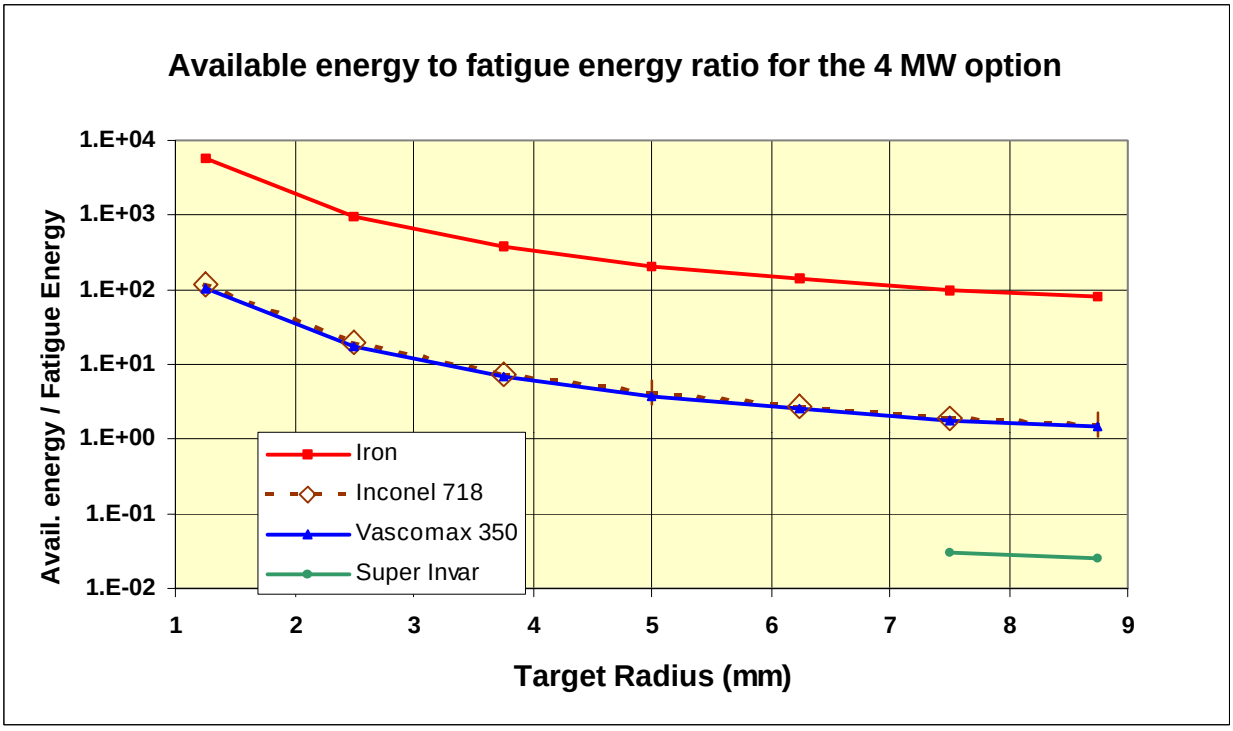
Available energy to fatigue energy ratio for the 4 MW option
Avail. energy / Fatigue Energy
1.E+04
1.E+03
1.E+02
1.E+01
1.E+00
1.E-01
1.E-02
1
2
3
4
5
6
7
8
9
Target Radius (mm)
Iron
Inconel 718
Vascomax 350
Super Invar

Fig. 10

The results for a 7.5 mm radius target and a 3 mm rms radius beam are summarized in Tables 4 and 5 for the 1MW and the 4 MW options respectively.

Table 4 1 MW-option results for a 7.5 mm radius target

	Iron	Inconel 718	Vascomax C- 350	Super Invar
Maximum Stress/ Yield Stress	1.7	0.27	0.16	0.025
Maximum Stress/ Fatigue Limit	3.3	0.48	0.47	0.050
Available Energy/ Yield Energy	10.9	0.28	0.09	0.004
Available Energy/ Fatigue Energy	43.6	0.87	0.81	0.014

Table 5 4 MW-option results for a 7.5 mm radius target

	Iron	Inconel 718	Vascomax C-350	Super Invar
Maximum Stress/ Yield Stress	3.4	0.54	0.32	0.05
Maximum Stress/ Fatigue Limit	6.7	0.95	0.94	0.10
Available Energy/ Yield Energy	24.2	0.61	0.21	0.008
Available Energy/ Fatigue Energy	96.8	1.93	1.79	0.03

One can see that iron is inadequate even for the 1 MW option, but the other three materials are probably viable, even for the 4 MW option. Only according to the most stringent criterion, (available energy/fatigue energy) could there be a problem in the 4 MW case with Inconel 718 and Vascomax C-350 for which these ratios are > 1. However, as was mentioned before, the fatigue endurance limits at high frequencies are expected to be considerably higher than the tabulated values used here. If these high-frequency values were known the computed energy ratios may well end up being <1. Another possibility for improving the situation even more is to use proton beams of non-Gaussian cross section. That possibility is discussed in the next section. The approach of simply adopting larger targets and correspondingly larger beams is limited by the increasing outgoing particle loss due to absorption.

Another observation is that Vascomax C-350 is superior to Inconel 718 if their respective yield stresses are considered, but they become almost equivalent if the fatigue endurance limit is take as the relevant factor.

Finally it is obvious from the Figs. 3 through 10 and from Tables 4 and 5 that Super Invar is vastly superior to the other materials regarding thermal shock, as long as the operating temperature doesn't exceed ~150 ^{0}C where the linear expansion coefficient starts to increase rapidly (see Fig.11). In Figs. 3 through 10 the curves corresponding to Super Invar do not extend to small radii because the higher energy density would heat the material too much. The assumption is that each portion of the target is thoroughly cooled to room temperature or below before returning to the reaction chamber. Important concerns regarding Super Invar are that rather careful heat treatments are required to achieve the very low values of the expansion coefficient, and it remains to be seen to which extent this property will be affected by repeated temperature cycling and by radiation damage. Experiments are planned[10)] to explore these questions.

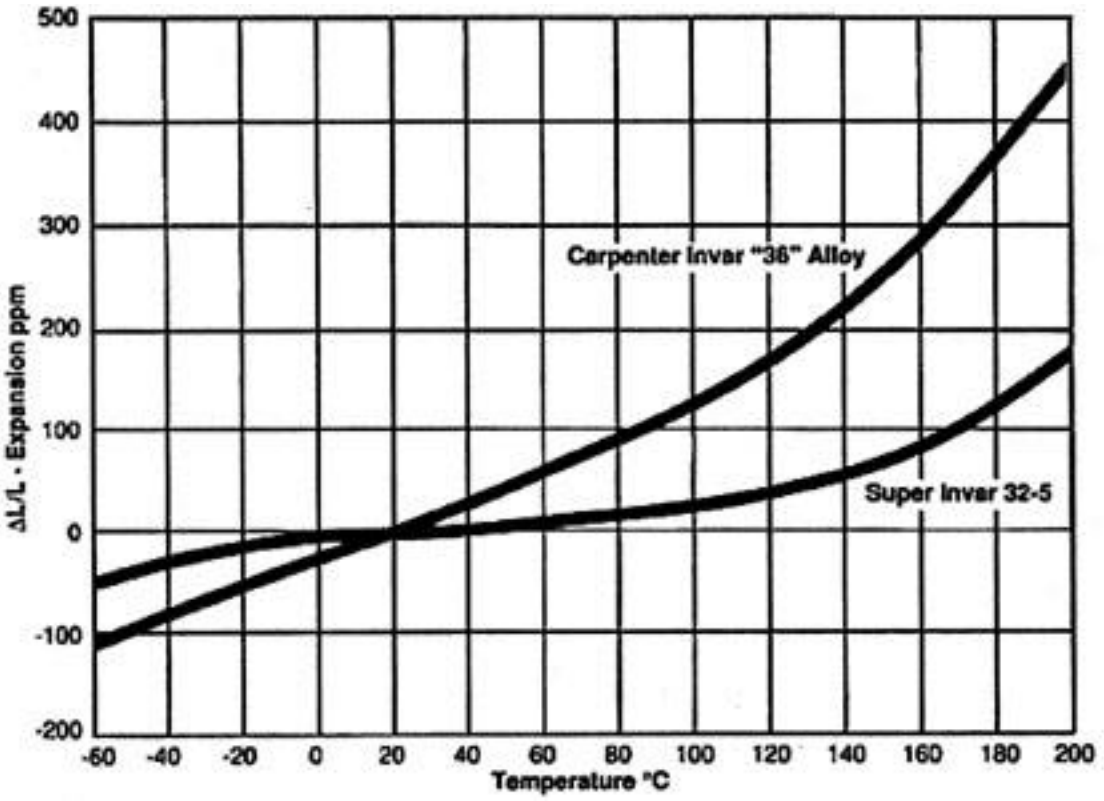

Fig. 11 Linear expansion as a function of temperature for Invar and Supper Invar alloys.

Non Gaussian Beams

One way to reduce maximum stresses is to reduce the peak energy density at the center of the target by spreading out the beam more uniformly over the target cross section. Ideally one would strive for a totally uniform beam, which, when compared to a Gaussian profile, would reduce the central energy density by a factor ~3 for a Gaussian beam with rms radius = 0.4 × target radius. The comparison of the intensity profile of such a "flat" beam with a Gaussian beam of equal total intensity is shown in Figs. 12a and 12b

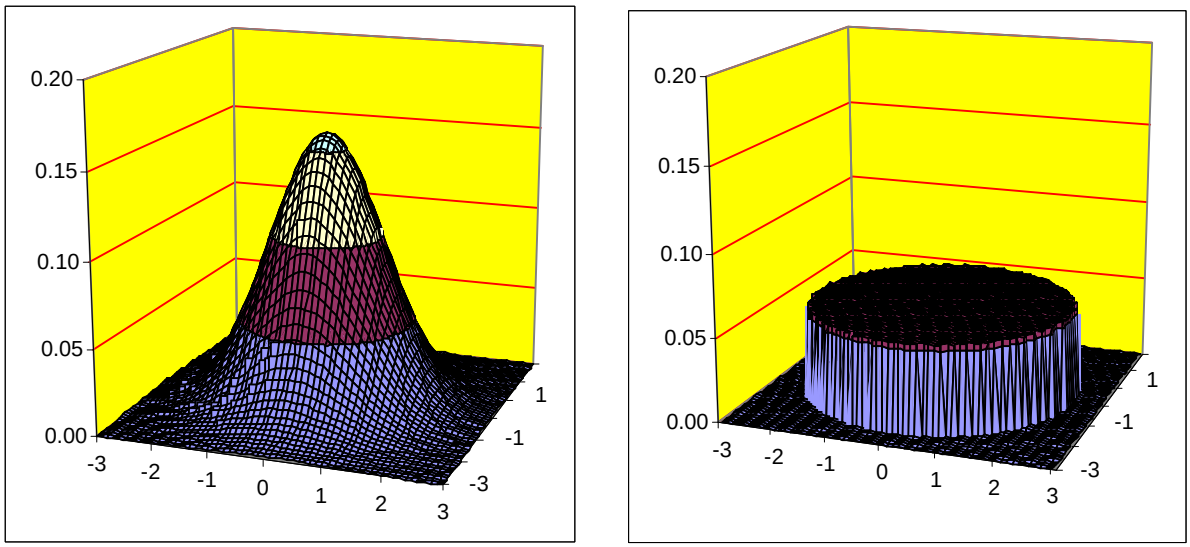

Fig 12a **Fig. 12b**

Comparison of a doubly Gaussian beam profile (a) with an ideal flat profile (b) containing the same number of particles.

A perfectly flat beam such as shown in Fig. 12b can of course not be realized, but using octupole lenses one can generate profiles which are fairly close to this goal. Fig 13 shows one of the projections of such a distribution which was calculated[11] for larger "uniform" beams required for the irradiation of biological materials.

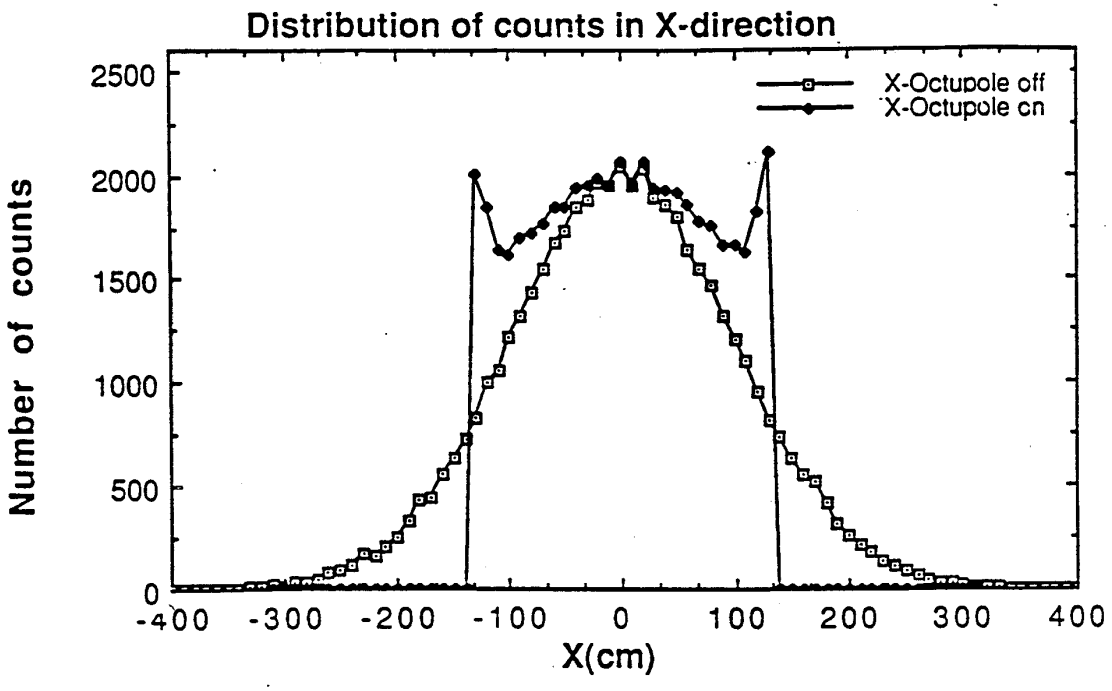

Fig. 13 Octupole-lens generated beam profile compared to a Gaussian profile with the octupole turned off.

While a factor of 3 in peak energy density reduction is out of reach, it seems reasonable to expect a factor ~2, which could be very significant (see Table 5)

One objection[12] to such non-Gaussian beams is that larger temperature gradients can induce unacceptably large thermal stresses. In our rather unique situation these stresses are however much smaller than the large dynamic stresses that can be induced following the inertially confined initial compression. This is discussed further below, in the section on residual stresses.

Stress Focusing

The stresses estimated in the previous sections can be exceeded in systems with highly symmetric geometries such as was observed[5] in simulations for circular windows rigidly constrained at the periphery and impacted by a circular beam centered on the window. In such a case reflected waves can interfere constructively generating large localized stresses before the oscillations die down. Similar calculations need to be performed for rod-shaped targets. If the problem appears then the solution will probably involve the selection of a cross-sectional shape without natural foci, i.e. circles and ellipses would need to be avoided. For example, rectangular cross sections such as suggested for the "band saw" target will probably work.

Possible Implementations

One possible implementation of a moving metallic target is the "Band Saw" system which has been previously described[13] . One potential disadvantage of that design is that the rigid circular target must enter and exit the extremely high radiation area at points where the radiation is still very high, and this fact leads to shielding difficulties. Also the geometry of the coils needs to be modified in a rather critical area to accommodate the "band saw".

Here we suggest the possibility of rather compact metallic chains such as sketched in Fig. 14 or the use of a metallic cable as originally suggested by Palmer [15] .

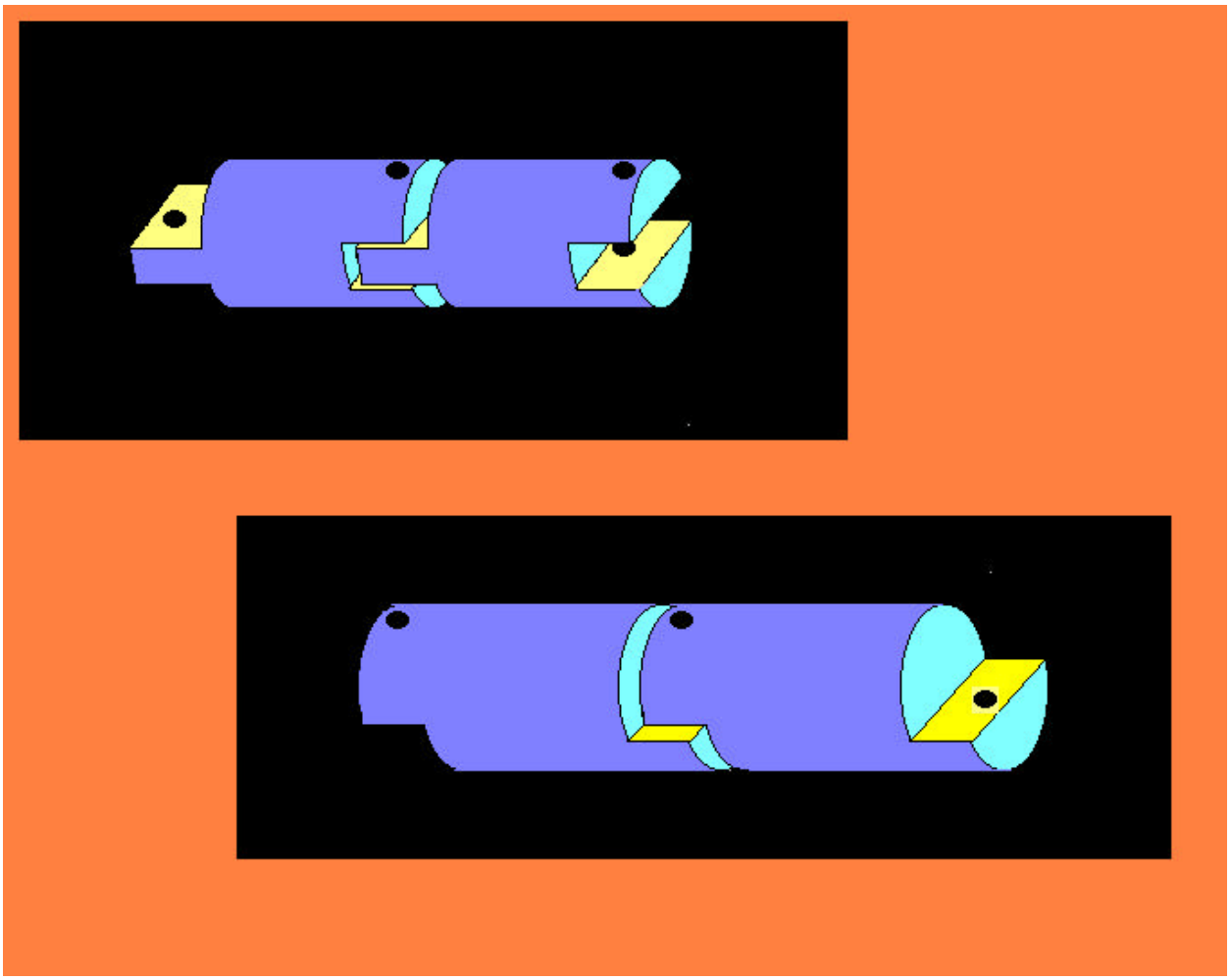

Fig. 14 Schematic examples of metallic chain links showing rather compact designs with large metal to gap volume rtatios.

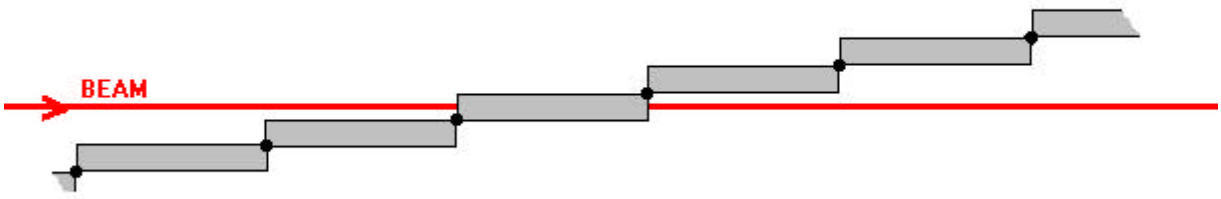

Fig.15 Schematic example of a chain with long links that would allow the beam to be coaxial with the target.

Such chains or cables could be as long as necessary to allow sufficient time for thorough cooling, and they could enter and exit the high radiation area at points sufficiently far removed from the reaction chamber so as to minimize the impact on shielding and on coil locations. In the case of chains, lubrication of the joints could be achieved with graphite powder or using graphite bushings. The reliability of such chains could be extremely high. We note that, in a different application, much lighter and weaker chains using plastic joints operate reliably for years at comparable velocities as part of the charging systems in many electrostatic accelerators[16].

To change such chains or cables, the old target can be used to pull the new one through, except in the unlikely event of an unexpected rupture. For such an eventuality it may be possible to leave in place auxiliary pull wires or cables which would not be exposed to the direct beam, and would therefore not be radiation damaged.

Finally, it should be mentioned that for most of these chain or cable configurations (except the one shown in Fig. 15), the beam would probably be inclined at a shallow angle with respect to the axis of the target. Nevertheless, all the stress estimates above, and also the cooling requirements estimated in the next section correspond to centered beams parallel to the target. The peak energy densities deposited by inclined beams are considerably smaller than assumed here. For such geometries we are therefore overestimating stresses and temperatures increments by up to a factor ~2, which is a nice safety factor.

Target Velocity and Length Considerations

The 1 MW and the 4 MW scenarios[1] considered as options for this project would have different pulse sequences and different beam intensities. These factors will obviously impact the choice of material and also the overall length and velocity of the target to avoid excessive heating and to allow sufficient time for cooling. The pulse sequences and intensities for both cases are represented schematically in Fig 16.

1 MW OPTION

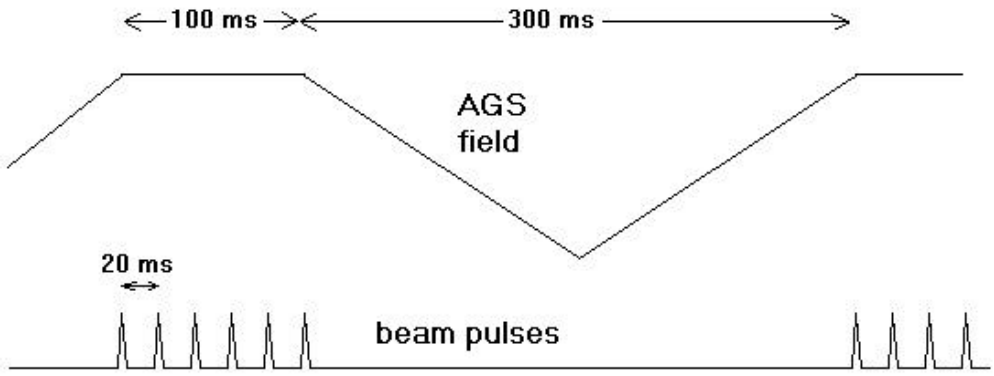

15 pulses per second
66.7 kJ per pulse
17.3 TP per pulse

4 MW OPTION

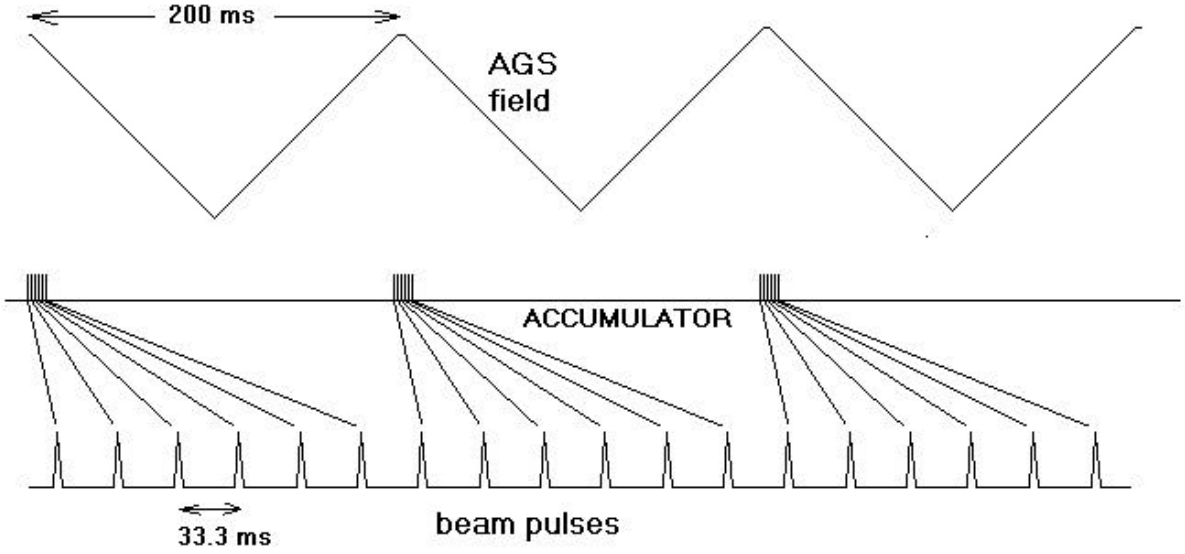

30 pulses per second
133 kJ per pulse
34.7 TP per pulse

Fig. 16 Proton beam pulse sequences for the proposed 1 MW and 4 MW options.

We first consider the case of Super Invar, using the example shown in Fig.2 for a 3mm rms radius beam impinging on a 7.5 mm radius target. Using the data for the 1MW and the 4 MW options shown in Fig.16 and the specific heat of Super Invar listed in Table 2, we obtain the core temperature increments along the 40 cm target shown in Fig.17

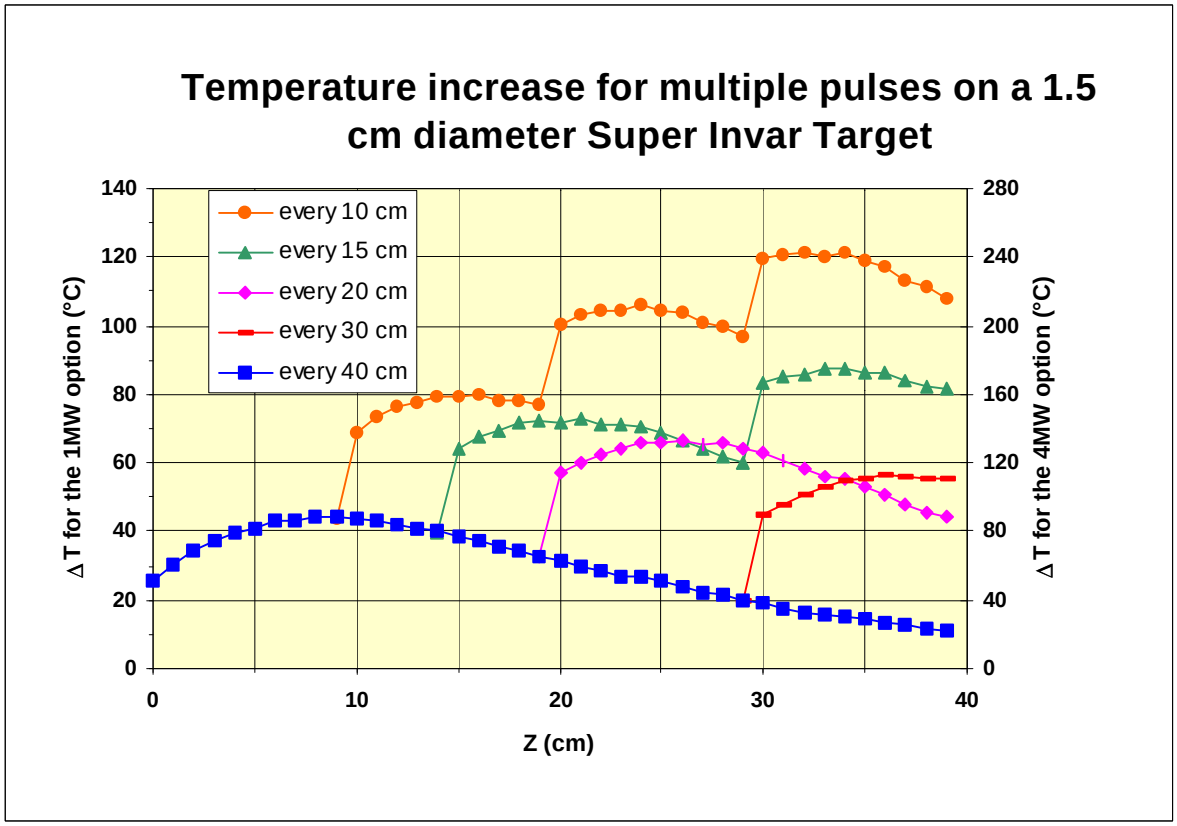

Fig. 17

The left temperature scale is for the 1 MW option and the right one for the 4 MW option. The lowest curve labeled "every 40 cm" corresponds to a single beam pulse per target section, avoiding any overlap. We see that for the 4 MW option the maximum temperature increment in this case is 86 ^{0}C. If the hottest spot in the target is cooled down to, say, 30 ^{0}C before returning to the reaction chamber then the maximum temperature reached could be 116 ^{0}C. In reality this temperature will be somewhat lower if the rotation of the chain or cable is such that the hottest spot from one cycle doesn't coincide with the maximum energy deposition point in the next cycle. In any case, considering the shape of the linear expansion coefficient curve (Fig. 11), one must conclude that overlapping of beam pulses must be avoided in this case. Then the minimum target velocity becomes 40 cm / 33.3 ms = 12.0 m/s which is one of the entries in Table 6 below.

For the 1MW option we can allow overlap. We see from fig. 17 that an acceptable ~87 ^{0}C degree increment is reached for the "every 15 cm" case. Accordingly the velocity entered in Table 6 for this case is 15 cm / 20 ms = 7.5 m/s.

Next we follow the same approach for Vascomax C-350. In this case we are less constrained in the allowable temperature increments since we don't rely on an abnormally low linear expansion coefficient of Super Invar which only holds over a very limited temperature range (see Fig. 11). Still we can't allow the material to become too hot because of the degradation with temperature of the mechanical strength. In Fig. 18 we show how the tensile strength varies with temperature. We presume that the fatigue endurance limit will vary in a similar fashion.

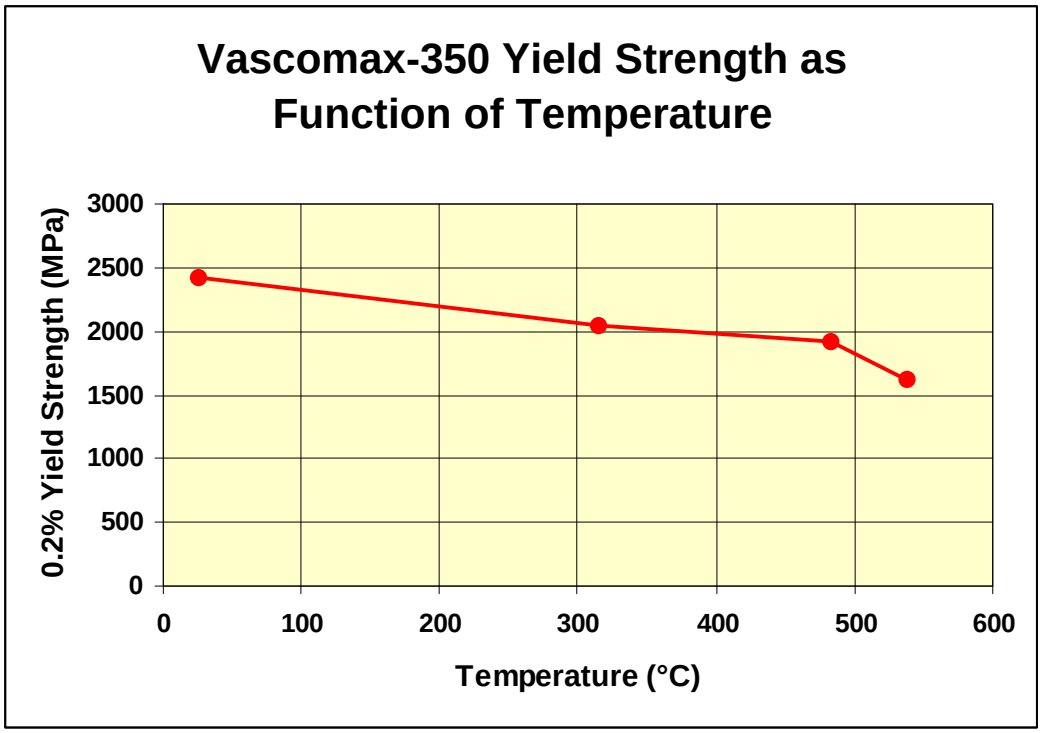

Fig. 18

For this discussion we arbitrarily assume that no more than 20% of the room-temperature value of the tensile stress must be lost and therefore, according to the data shown in Fig. 18, a maximum of 300 ^{0}C temperature increment is allowable.

The results of the maximum temperature increase calculations for Vascomax C-350 are shown in Fig. 19

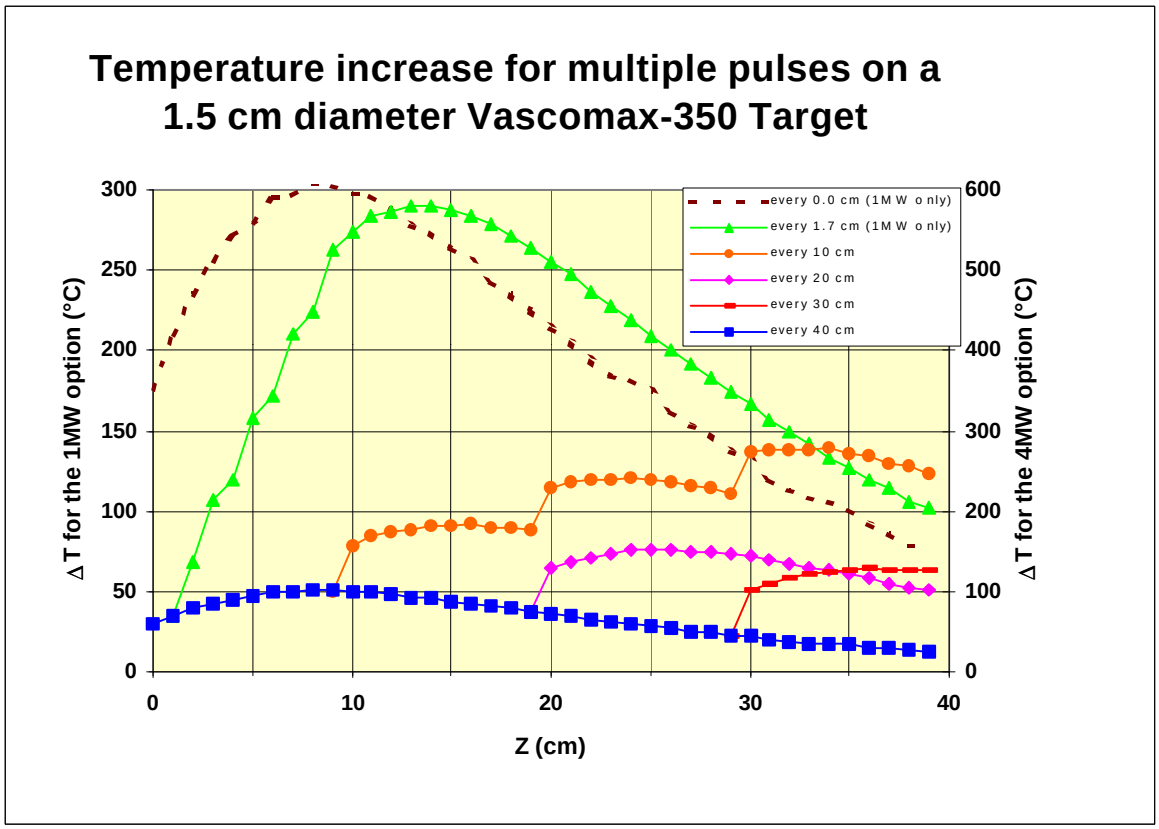

Fig. 19

Here the uppermost two curves correspond to the 1 MW option only, taking advantage of the intermittent sequence of six pulses during 100 ms followed by a 300 ms pause. For the curve labeled "every 0.0 cm" the target is stationary for the 6-pulse sequence (see Fig. 16), and then advances by one target length (40 cm) during the 300 ms interval. This mode would be particularly advantageous for a target made of 40 cm long links such as the one sketched in Fig. 15. The curve labeled "every 1.7 cm" moves continuously just fast enough (1.7 cm/ 20 ms = 0.85 m/s) to get a fresh portion of the target into position at the beginning of the next 6-pulse burst. We see that in both cases we stay within the ~300 ^{0}C limit established above. For the 4 MW option we can go up to one pulse every 10 cm (10cm / 33.3ms = 3 m/s) to stay below the 300 ^{0}C increment.

We now summarize these examples in Table 6:

Table 6. Examples of target velocities and lengths according to assumptions explained in the text.

	Velocity (continuous motion)	Minimum length (continuous motion)	Average Velocity (intermittent motion)	Minimum length (intermittent motion)
	m/s	m	m/s	m
Super Invar - 1 MW Option	7.5	175		
Vascomax C-350 - 1 MW Option	0.85	16.8	1.0	18
Super Invar - 4 MW Option	12.0	274		
Vascomax C-350 - 4 MW Option	3.0	34		

The minimum target lengths were estimated from the velocities by assuming the chain or cable travels through the cooling bath for the characteristic 1/e cooling time (Table 1) which is 22 s for Invar and 8 s for Vascomax C-350. It

was further assumed that there is a minimum 10 m of target outside the bath. The need for the much longer Invar target chains arises from the higher velocities required to keep the temperature in a narrow interval, combined with the lower heat conductivity requiring longer cooling. These length estimates can vary rather considerably with better heat transport calculations based on actual chain geometries. Also the shorter Vascomax C-350 lengths may not be adequate if one wants to extend the life of the chains by spreading radiation damage over large total volumes.

Eddy Currents and Magnetic Forces

Eddy currents will be induced in conductors moving through magnetic field gradients. These currents will cause some heating and will also give rise to forces opposing the motion. Additional large forces will be present when a ferromagnetic material such as Vascomax C-350 enters and exits a 20T solenoidal magnetic field. We will estimate these effects for the worst case example listed in Table 6, namely a 1.5 cm diameter cylindrical Vascomax C-350 target moving at 12 m/s. We will limit this discussion to on-axis motion to obtain orders of magnitude of the forces involved, recognizing that more complex situations, including forces perpendicular to the target, will occur for inclined targets and for portions of the target moving over pulleys.

For the present calculations we use the axial magnetic field profile depicted in Fig. 20 calculated for a 20T solenoidal field generated by an array of superconducting coils, followed by a region where the field, shaped by additional coils, gradually tapers off. For the present example we (somewhat arbitrarily) consider a ~5m long target cylinder starting 1 m before the solenoid exit plane.

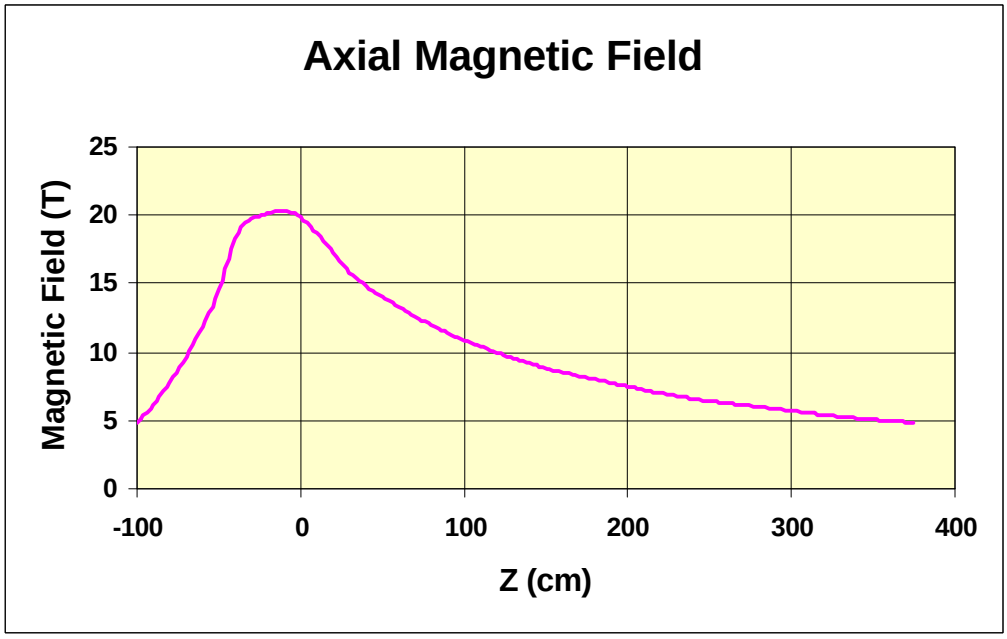

Fig. 20 Axial magnetic field calculated for the 20T solenoid arrangement described in the Feasibility Study[1)].

To calculate de Eddy currents and the forces they generate we use equations developed for these quantities during a previous study[17)] of the behavior of a mercury jet entering a magnetic field:

$j = -\sigma r/2c \; V_z \; \delta B_z/\delta z$

where j is the current density at a radius r, σ is the conductivity, c the velocity of light and V_z the velocity of the target and,

$f_z = -\sigma r^2/4c^2 \; V_z \; (\delta B_z/\delta z)^2$

where f_z is the axial force density due to the interaction of the Eddy current with the field.

We evaluate these quantities as well as the derived power density σj^2 and temperature increase using the values for Vascomax C-350 in Gaussian units shown in Table 7:

Table 7. Values in Gaussian units used in the calculations for a Vascomax C-350 target

Electrical conductivity σ	1.023E+16 1/s
Density ρ	8.08 g/cm^3
Specific Heat	4.50E+6 erg/(gK)
Saturated Magnetization	1.86E+4 Oersteds
Target velocity V_z	1200 cm/s
Light velocity c	3E+10 cm/s

The results are shown in figs. 21, 22 and 23

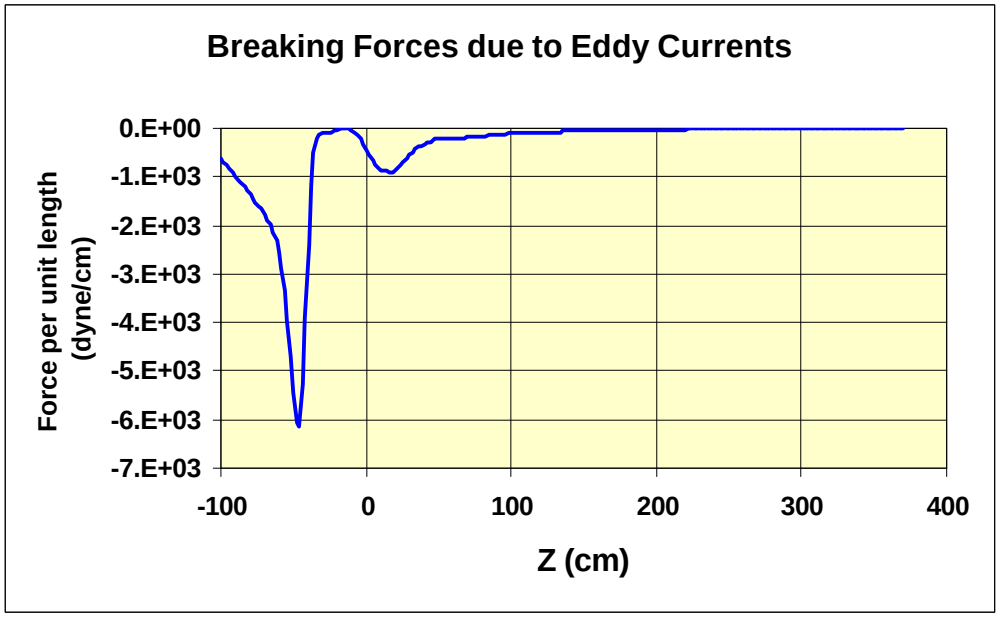

Fig. 21 Breaking forces per unit target length due to Eddy currents in a 1.5 cm diameter Vascomax C-target moving axially at 12 m/s through the field shown in fig. 20.

We can see that the forces due to eddy currents are small. The total force obtained by integrating the values shown in fig. 21 is 1.99 Newtons or 0.2 kg force. The total power dissipation due to these currents is 6 W and the maximum temperature increase is only ~ 6×10^{-3} ^{o}C.

In contrast, the magnetic forces on Vascomax C-350 which is a ferromagnetic material are rather large:

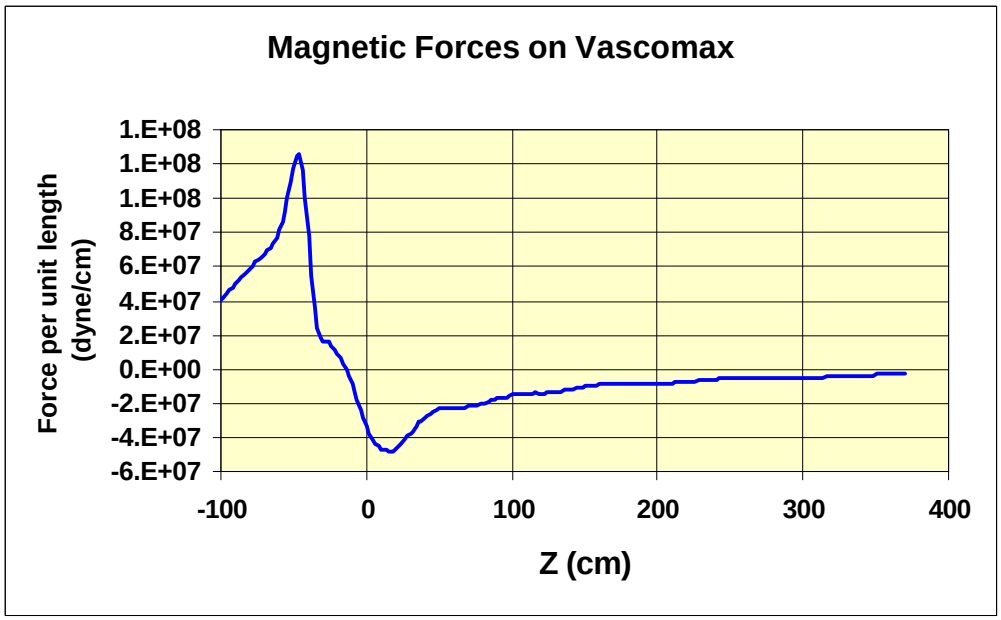

Fig. 22 Magnetic forces on a 1.5 cm diameter Vascomax C-350 target placed in the field shown in fig. 20.

We can see that, as expected, these forces tend to pull the material into the high field region of the solenoid. For this 1.5 cm diameter Vascomax C-350 target, the force per unit length reaches a maximum of 12.5 Newton/cm or ~1.3 kg force per cm. To maintain the chain or cable under tension everywhere we must apply external tension. An example of this is shown in fig.23 where an external ~3.9 MPa tension was applied to maintain a minimum of 1 MPa at the maximum field point. The actual value of the required external tension will depend on the desired trajectory of the target and on the maximum allowable deviation from a straight line. In the case of an inclined target such deviations will be due to transverse components of the magnetic forces and to a smaller extent to gravity.

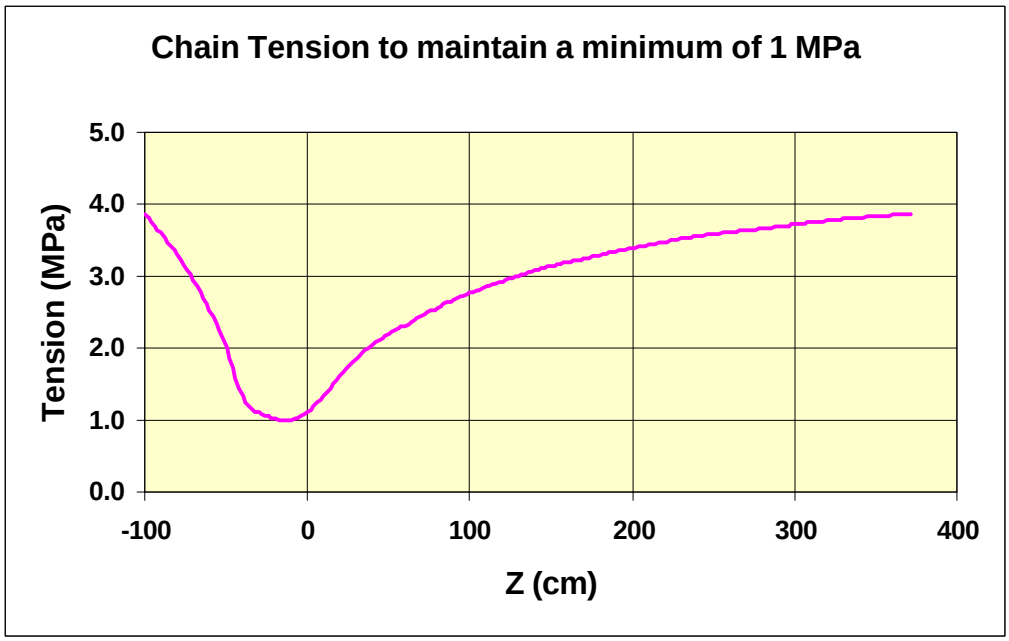

Fig. 23 Tension as a function of position for a 1.5 cm diameter Vascomax C-350 target placed in the field shown in fig.20. In this example, an external tension is applied to achieve a minimum tension of 1 MPa.

Tensions of ~4 MPa such as shown in fig. 23 are negligible when compared to the yield strength (~2200 MPa), but they may complicate the engineering and required lubrication of the bearings joining the links of such a chain. The force corresponding to this tension is ~707 Newton or ~71 kg force. This is one more reason, in the case Vascomax C-350 is used, why a cable[15)] may be preferable to a chain.

Residual Stresses

After the strong vibrations following each beam pulse subside there will still be a non-uniform temperature distribution present in the target, causing residual stresses which will later disappear on a longer time scale (see Fig. 1). In the cases where multiple successive pulses impinge on the same portion of the chain or cable, pulses subsequent to the first one will encounter already stressed material, and the transient vibrational stresses will be superimposed on residual stresses. The worst such case contemplated above was the one depicted as the dotted curve in fig. 19 for Vascomax C-350. Here six pulses spaced by 20ms (see fig. 16) hit a 7.5 mm radius stationary target leading to a maximum on-axis temperature increment of ~300 ^{0}C. Taking into account the radial dependence of the energy deposition (fig. 2) at Z= 9 cm, and the specific heat of the material, we calculate de temperature distribution after 5 pulses, and from these values we obtain the residual stresses that will be encountered at the arrival of the 6th pulse. The results of this calculation are shown in Fig. 24

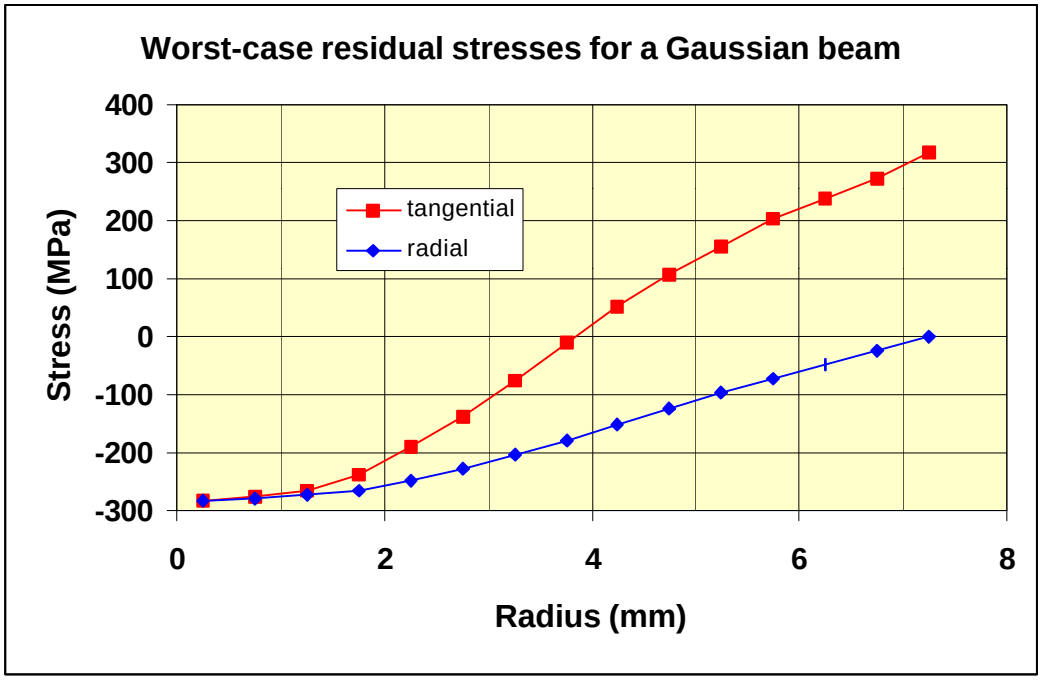

Fig. 24

The same approach was followed as we previously used for carbon rods [4)] using thermal stress equations [18)] for cylindrical geometry with arbitrary radial temperature profiles. In this figure compression is indicated by positive stress values and tension by negative values. We see that even in this worst case, the residual stresses are not very significant when compared to the yield stress or to the fatigue endurance limit.

For the "flat" beam case (Fig. 12b) we get similar residual tangential stress values as can be seen from fig. 21 below:

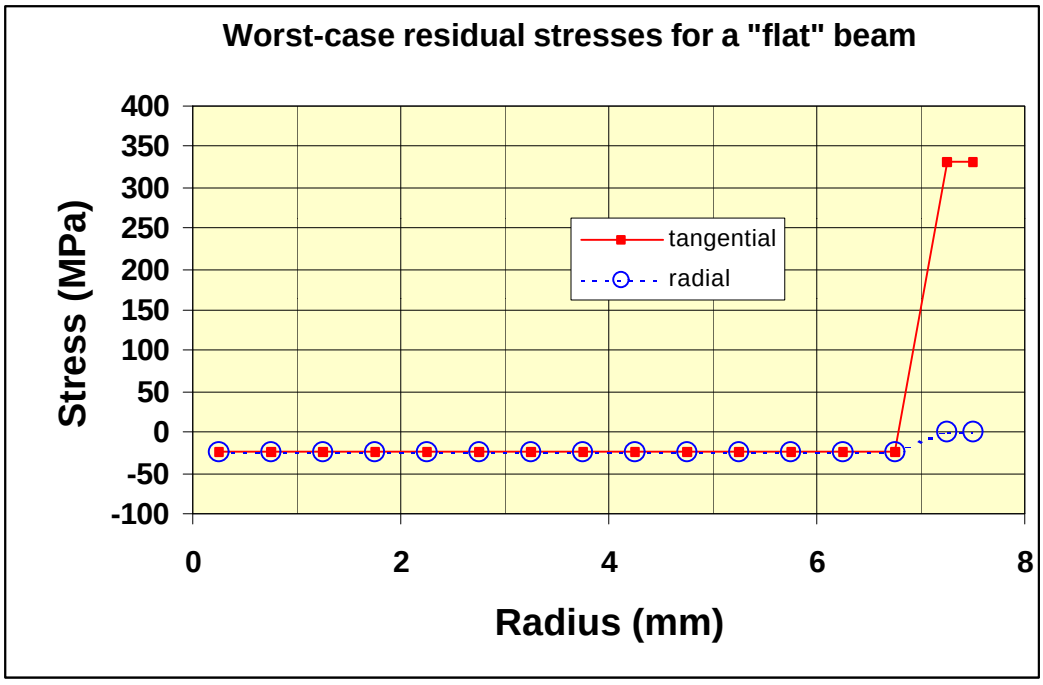

Fig 25

Here we assumed that the same total beam energy density at z=9 cm is uniformly distributed within a 7 mm radius circle leaving a 0.5 mm wide un-irradiated annular sheet. Since the residual stresses aren't any worse, one could take full advantage of the reduced transient stresses discussed before.

Questions about Invar

The small linear expansion coefficients of these materials seems to continue puzzling the specialists, even though progress has been made over the years. One question that came up regarding our possible application is the time response of the material given the short pulse lengths involved. In other words does the small expansion result from a larger expansion followed by a later contraction or vice versa. Or are such processes (if they exist) much faster than our time scale. After consulting a specialist in this field[19)] we obtained the following answer:

"The Invar effect is a strong magneto-volume coupling effect, and therefore, the time scales in which the effect actuates correspond to lattice fluctuation times in the order of 10(-13 s). 10 ns is too long compared to this time scale, so that the overall thermal expansion would still be valid."

This answer suggested the next question. Namely, if the Invar effect is a "magneto-volume coupling effect", will the response be modified by the presence of a strong external magnetic field such as we will have in our system. Fortunately that question had been answered experimentally by H. Zähres. M.Acet, W. Stamm and E.F. Wassermann[20)] for fields up to 6 Tesla . We reproduce part of their results in fig. 26:

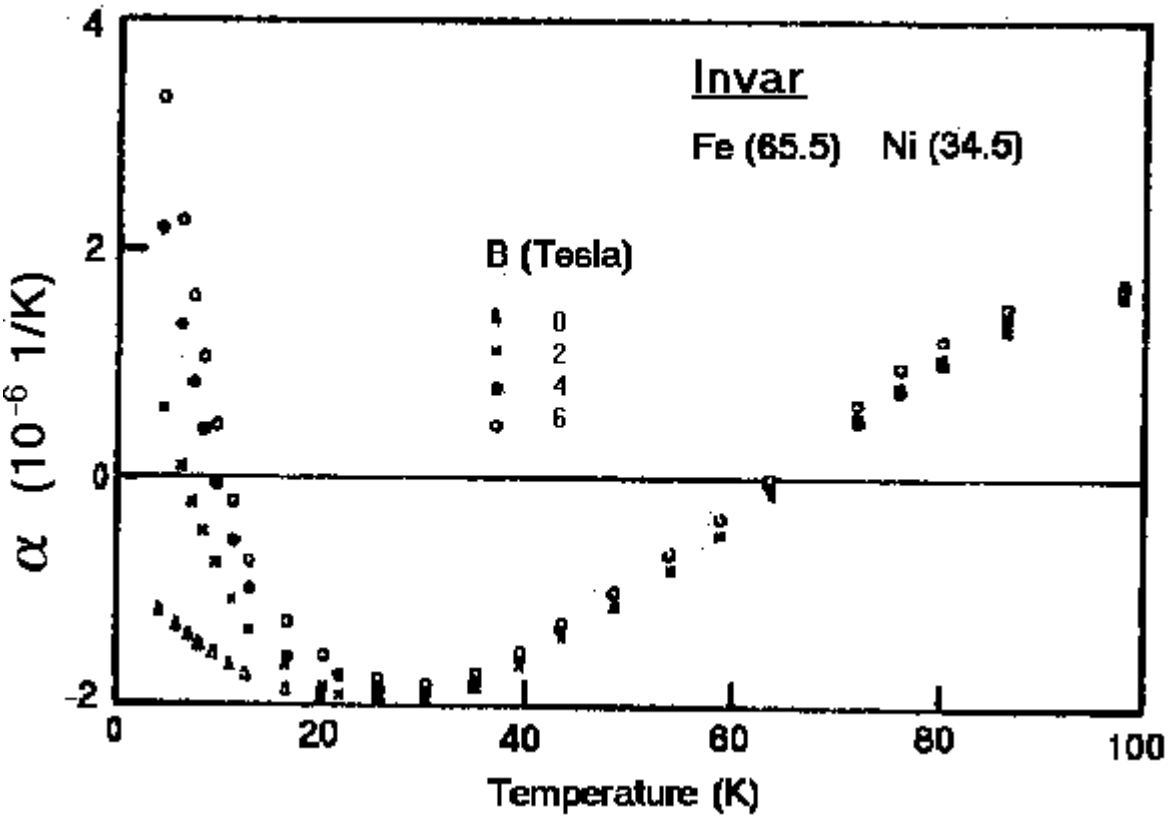

Fig. 26 Invar linear expansion coefficient as a function of temperature and magnetic field [19].

We see that there is a pronounced magnetic effect on the linear expansion coefficient at cryogenic temperatures up to about 30 K, but that effect disappears at higher temperatures. These experiments were done with Invar. We presume that Super Invar will show a similar behavior. In Fig. 27 we compare these data (left side of the figure) with an approximate representation of the known expansion coefficient values around room temperature, both for Invar and for Super Invar.

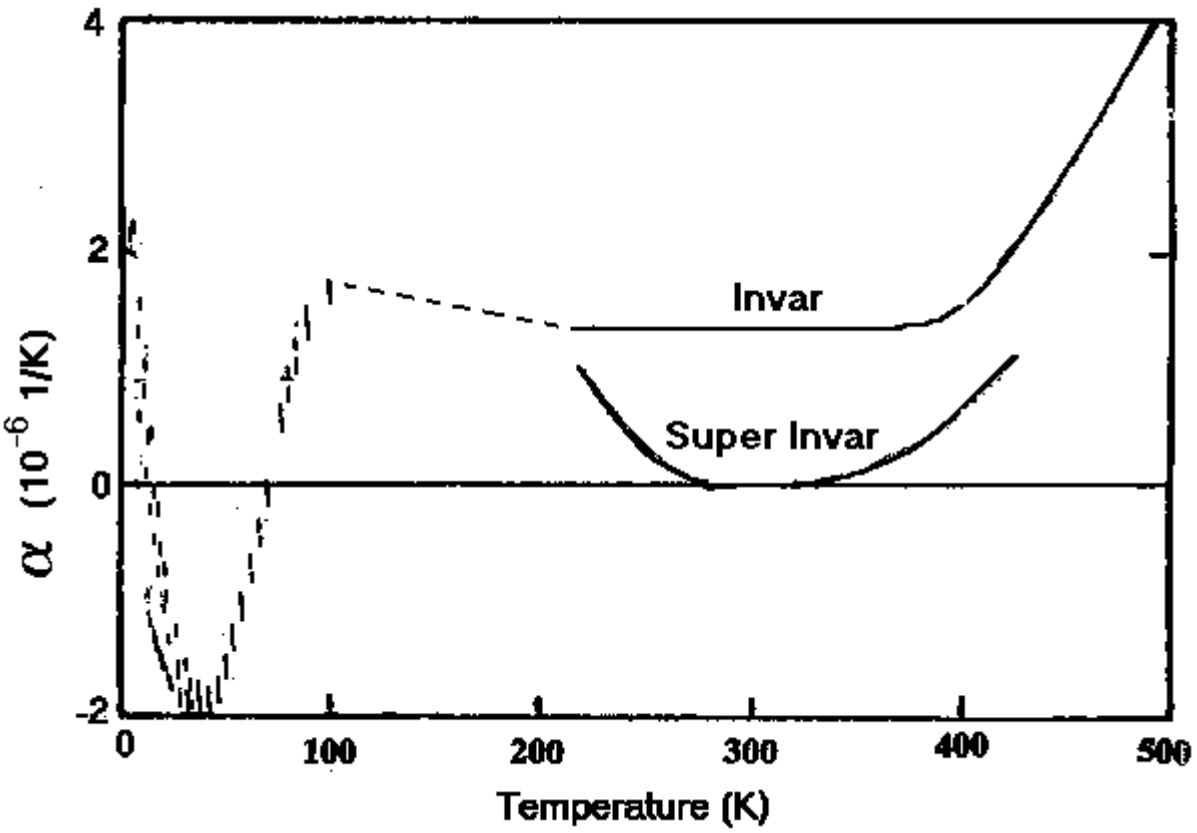

Fig. 27 Low temperature data[20] from Fig. 26 combined with known expansion coefficients at higher temperatures.

We conclude that neither time response limitations nor magnetic effects would affect the usefulness of super invar for our application..

Discussion and Conclusions

Special solid metallic targets with very large tensile strength or with very low coefficients of expansion are viable candidates for the 1 MW option, and very probably also for the 4 MW option. It was also shown that more conventional solids such as iron can not be expected to work at all. This may help to explain the rupture of some metallic targets at CERN[21] which probably led to the prevailing pessimism regarding solid targets for this application.

The present stress and temperature estimates are very conservative since no credit was taken for the beneficial effects of inclined beam incidence on the target, nor for the advantageous frequency dependence of fatigue tolerance, nor for the possibility of using non-Gaussian beam profiles. As was discussed before[4] special forms of graphite my also work. It seems therefore that the complications and uncertainties associated with mercury jets[3] can be avoided.

The advantage of the graphite option is that a stationary target is simple and reliable since moving parts are avoided. Disadvantages are the 50% yield loss compared to heavy targets, the fact that a cooled jacket will line the chamber taking up some of the volume otherwise available to the spiraling particles, and that the highest radiation dose will be constantly delivered to the same volume element of the target probably leading to premature failure due to radiation damage.

The advantages of the metallic targets discussed here are that most of the yield available for mercury targets will be realized[14], that the radiation damage will be much more spread out and that target cooling can take place outside the reaction chamber, far away from the very high radiation environment. The disadvantage is the complication and potential reliability problems with moving mechanical parts.

The thermal shock advantage of Super Invar over Vascomax C-350 can only be realized with thorough cooling between beam exposures. This together with the lower heat conductivity of Super Invar leads to much longer total target chains. If Vascomax C-350 survives the repeated thermal shock (and we have seen that there is an excellent chance that it will) it may become the preferred option. Inconel 718, while similar to Vascomax C-350 in its fatigue endurance, shares the lower heat conductivity of Super Invar. For Vascomax C-350 the chain length may have to be increased beyond minimum values required for cooling in order to spread radiation damage over a larger volume to extend the lifetime of the chain. The Vascomax C-350 chain may thus become long enough to match the minimum length requires for cooling a Inconel 718 chain of cable. In this case Vascomax C-350 and Inconel 718 become equivalent assuming their radiation-damage rates are similar. Inconel 718 may then be preferable to avoid possible problems associated with large magnetic forces. The main comparative advantages and disadvantages of the three solid metallic targets are summarized in Table 8:

Table 8. Comparison of advantages and disadvantages the three alloys considered in this paper.

MATERIAL	ADVANTAGES	DISADVANTAGES
Super Invar	Largest margin for thermal shock tolerance. Absence of large magnetic forces.	Narrow temperature range and low heat conductivity leading to the need for long chains or cables. The largest uncertainty regarding deleterious effects of radiation damage.
Vascomax C-350	Largest tensile strength. Good heat conductivity allowing the use of relatively short chains or cables.	The material is ferromagnetic and will be subject to large magnetic forces
Inconel 718	Good fatigue endurance limit similar to Vascomax C-350. Absence of large magnetic forces.	Poor heat conductivity (similar to Super Invar) requiring long chains of cables, but not as long as for Super Invar since the temperature range is not as small.

These three alloys appear to be viable candidates for targets in a future Muon Collider or Neutrino Factory. Radiation damage studies[10] as well as further experiments, more detailed simulations, and engineering considerations will help in the selection of one of these materials.

Appendix

We derive here the expressions used in equations 3, 4 and 5 to calculate P_{max}, the maximum pressure following beam heating , E_σ, the energy densities required to reach the yield stress or the fatigue endurance limit, and E_m the energy density available in the initially compressed volume element, respectively.

Calling ε_{max} the maximum total energy density (per unit mass) deposited by the beam in a volume element V_0 of the target of density ρ , and c_v the specific heat at constant volume of the target material, the temperature increase ΔT_{max} of that volume element will be:

$$\Delta T_{max} = \varepsilon_{max} / c_v \qquad (6)$$

If we allowed V_0 to expand freely it would occupy a volume $V_1 = V_0 + \Delta V$ where

$$\Delta V = 3\,\alpha \times \Delta T_{max} \times V_0 \qquad (7)$$

α being the linear expansion coefficient.
Before V_1 expands, the compression is therefore $\Delta V / V_0$ and the pressure is:

$$P_{max} = B \times \Delta V / V_0 \qquad (8)$$

where B is the bulk modulus. From 6), 7) and 8, we get the equation we used before for the maximum pressure:

$$P_{max} = 3 \times \varepsilon_{max} \times B \times \alpha / c_v \qquad 3)$$

We now turn to the mechanical energy density, E_{σ}, contained in a volume element stressed to a stress σ. For that purpose we imagine a rod of initial length x_0 and cross-section s, stretched to a length x by applying a force F(x) to one end:

$$F(x) = Y \times s \times (x - x_0) / x_0 \qquad 9)$$

Where Y is the Young modulus. The work W done to reach x starting form x_0 will be:

$$W = \int_{x_0}^{x} F(x)\,dx = 1/2\ Y \times s \times (x - x_0)^2 / x_0 \qquad 10)$$

If $(x - x_0)/x_0$ is the strain corresponding to the stress σ then:

$$(x - x_0)/x_0 = \sigma / Y \qquad 11)$$

and the work W_{σ} to reach this strain is from (10) and (11):

$$W_{\sigma} = 1/2 \times Y \times s \times (x_0 \times \sigma / Y)^2 / x_0 \qquad 13)$$

But $x_0 \times s$ is the volume. Therefore the energy per unit mass is:

$$W_{\sigma} / (x_0 \times s \times \rho) = E_{\sigma} = \sigma^2 / (2\,Y\,\rho) \qquad (4)$$

Which is the expression for the energy per unit mass used before for $\sigma = \sigma_{0.2}$ (the yield stress) or $\sigma = \sigma_{-1}$ (the fatigue endurance limit), to compare with the maximum mechanical energy density available.

We finally will derive the expression used to calculate that maximum mechanical energy density E_m available in the initially inertially confined compressed volume. This mechanical energy will be only a fraction of the total maximum energy ε_{max} deposited by the beam, most of which goes directly into heating the material.

As the first step we calculate the temperature decrease ΔT when we allow a volume element of initial density ρ_0, temperature T_0 and pressure P_0 to expand adiabatically. We do this in two imaginary steps:

First we remove some heat ΔQ_1 at constant volume obtaining a temperature T_1 and pressure P_1

$T_1 = T_0 - \Delta T_1$
$\Delta T_1 = \Delta Q_1/c_v$
$P_1 = P_0 - \Delta P_1$

Now we add some heat ΔQ_2 at constant pressure:

$\Delta T_2 = \Delta Q_2/c_p$ $\quad$ $T_2 = T_0 - \Delta T_1 + \Delta T_2$

The volume increases by:

$\Delta v = 3\,\alpha \times v \times \Delta T_2$ $\quad$ 14)

Where v is the specific volume ($1/\rho$) and α the linear expansion coefficient
Setting $\Delta Q_1 = \Delta Q_2$ to get an overall adiabatic expansion we get:

$c_v\,\Delta T_1 = c_p\,\Delta T_2$
$\Delta T_1/\Delta T_2 = c_p/c_v$
$(\Delta T_1 - \Delta T_2)/\,\Delta T_2 = (c_p - c_v)/c_v$
$\Delta T_2 = (\Delta T_1 - \Delta T_2)\,c_v\,/\,(c_p - c_v) = 1/(3\,\alpha)\;\; \Delta v/v$ $\quad$ from 14) above we get
$\Delta T = \Delta T_2 - \Delta T_1 = -\,(c_p - c_v)/c_v \;\; 1/(3\,\alpha) \;\; \Delta v/v$ $\quad$ or $\quad$ $dT = -\,(c_p - c_v)/c_v \;\; 1/(3\,\alpha) \;\; dv/v$ $\quad$ 15)

for an infinitesimal adiabatic expansion.

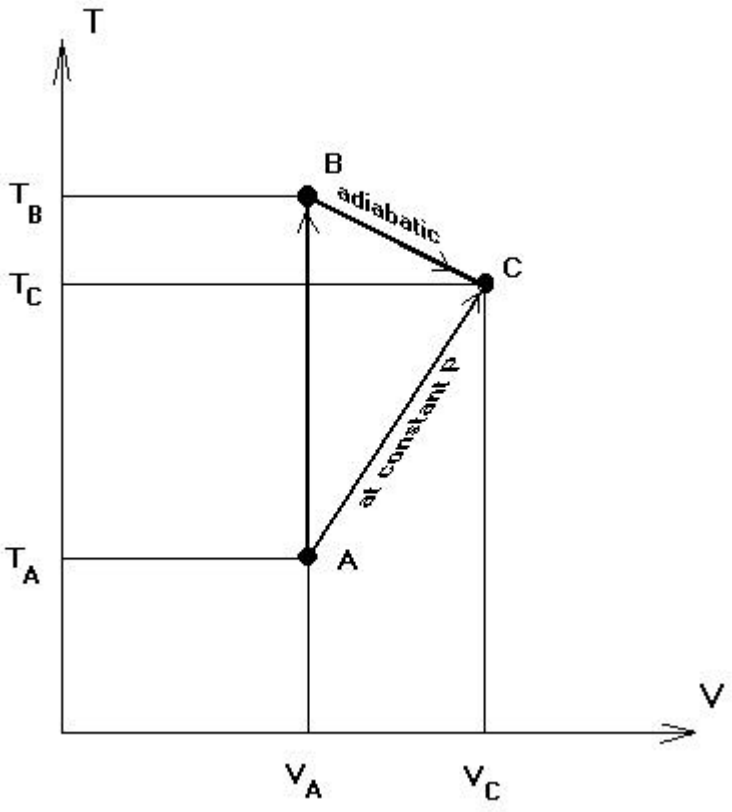

Fig. 28 Diagram used to calculate the mechanical energy released during an adiabatic expansion following inertially confined heating of the target (see text).

We now use the diagram of fig. 28 to plan the calculation of the mechanical energy released during the adiabatic expansion (B → C) following the inertially confined heating of the target by the beam (A → B). The final point C could in principle also be reached by heating at constant pressure (A → C). We will calculate the total energies per unit mass E_{AB} and E_{AC} required to go from A to B and from A to C respectively. The difference $E_{AB} - E_{AC}$ will be the energy released from B to C. Since this is an adiabatic transition, there is no heat exchange and this energy E_{BC} is therefore entirely mechanical.

$$E_{BC} = \int_{Ta}^{Tb} c_v \, dt - \int_{Ta}^{Tc} c_p \, dt = \int_{Ta}^{Tc} (c_v - c_p) \, dt - \int_{Tc}^{Tb} c_v \, dt \qquad 16)$$

We know that [17] :

$$c_p - c_v = v \; T \; B \; \alpha^2 \qquad 17)$$

and therefore the first term becomes:

$$v \; B \; \alpha^2 \; (T_c^{\,2} - T_a^{\,2}) / 2 \qquad 18)$$

To calculate the second term we use (15) and the fact that:

$$\Delta v/v = (v_c - v_a) / v_a = 3 \; \alpha \; (T_c - T_a) \qquad 19)$$

$$T_B - T_C = - (c_p - c_v)/c_v \;\; 1/(3 \; \alpha) \;\; 3 \; \alpha \; (T_c - T_a) \qquad 20)$$

Since $T_B - T_C << T_B - T_A$ we can use 17) to substitute the value $c_p - c_v$ at T_C:

$$T_B - T_C = - (v \; T_c \; B \; \alpha^2) / c_v \;\; (T_c - T_a) \qquad 21)$$

Assuming $c_v \approx$ constant over the small temperature interval $T_B - T_C$ we get the second term of 16):

$$v \; T_C \; B \; \alpha^2 \; (T_c - T_a) \qquad 22)$$

Combining 18 and 22:

$$E_{BC} = v \; B \; \alpha^2 \; (T_c^{\,2}/2 - T_a^{\,2}/2 + T_c^{\,2} - T_c \; T_a) \qquad 23)$$

Approximately $T_c \approx T_a + E_{AB} / c_p$ and we get:

$$E_{BC} \approx E_{AB} \; v \; B \; \alpha^2 \;\; (2 \; T_a + 3/2 \;\; E_{AB}/c_p) / c_p \qquad 24)$$

Which is equivalent to (5) used in the text.

Acknowledgements

We would like to acknowledge stimulating discussions with R.J. Weggel, N. Simos R. B. Palmer. And K. McDonald. R.J. Weggel suggested the investigation of Vascomax C-350 as one of the strongest materials available.

References

1. N. Holtkamp and D. Finley: editors, A Feasibility Study of a Neutrino Factory Based on a Muon Storage Ring, http://www.fnal.gov/projects/muon_collider/nu-factory/
2. AGS experiment E951
3. P. Thieberger, MUC note# 212: http://www-mucool.fnal.gov/mcnotes/muc0212.pdf
4. P.A. Thieberger and H.G. Kirk, MUC note (to be published)
5. Simos windows modeling.
6. Cylindrical targets are assumed here for simplicity even though the final design may be different if stress-focusing effects are significant.
7. Handbook of Physical Quantities, I.S. Grigoriev and E.Z. Meilikhov, Editors, CRC Press, Inc. 1997, page 179.
8. N.V. Mokhov and A. Van Ginneken, Pion Production and Targetry at mu+mu- Colliders, Fermilab-Conf-98/041 (Jan. 1998).
9. N.V. Kadobnova and A.M. Bratkovskii, Handbook of Physical Quantities, I.S. Grigoriev and E.Z. Meilikhov, Editors, CRC Press, Inc. 1997, page 83.
10. Radiation Damage experiments to be performed with 200 MeV protons.
11. N. Tsoupas in Booster Applicatins Facility Report,Phase II - BNL-52291
12. N. Simos and R.J. Weggel, private communication
13. B.J. King, N.V. Mokhov, N. Simos and R.V. Weggel, April 9,2001, http://pubweb.bnl.gov/users/bking/www/papers/
14. N.V.Mokhov, Private communication to N. Simos
15. R.B. Palmer, private communication.
16. Pelletron chain charging system. National Electrostatics Corporation, Middleton, Wisconsin.
17. P.Thieberger, MUC note #0182: http://www-mucool.fnal.gov/mcnotes/muc0182.pdf
18. Elements of Thermal Stress Analysis, David Burgreen, C.P. Press 1971, pages 246 and 251.
19. M.Acet, Tieftemperaturphysik, Universität Duisburg, Germany, private communication.
20. H. Zähres. M.Acet, W. Stamm and E.F. Wassermann, Journal of Magnetic Materials 72 (1988) 80-84
21. H. Haseroth, private communication.